# NACA

# RESEARCH MEMORANDUM

EXPERIMENTAL INVESTIGATION OF PERFORMANCE OF

SINGLE-STAGE TRANSONIC COMPRESSOR WITH

GUIDE VANES TURNING COUNTER TO

DIRECTION OF ROTOR WHIRL

By Lawrence J. Jahnsen and Theodore E. Fessler

Lewis Flight Propulsion Laboratory
Cleveland, Ohio

# NATIONAL ADVISORY COMMITTEE
# FOR AERONAUTICS

NATIONAL ADVISORY COMMITTEE FOR AERONAUTICS

RESEARCH MEMORANDUM

EXPERIMENTAL INVESTIGATION OF PERFORMANCE OF SINGLE-STAGE

TRANSONIC COMPRESSOR WITH GUIDE VANES TURNING

COUNTER TO DIRECTION OF ROTOR WHIRL

By Lawrence J. Jahnsen and Theodore E. Fessler

## SUMMARY

A transonic compressor rotor with double-circular-arc blade sections and inlet guide vanes turning counter to the direction of rotor whirl was designed and tested to determine the effect of blade-row interaction on the performance of a transonic rotor. The compressor was designed for a pressure ratio of 1.35 and a corrected specific weight flow of 31.5 pounds per second per square foot of frontal area at a corrected tip speed of 1000 feet per second. Over-all and blade-element performance and circumferential survey results are presented.

The over-all performance of this rotor was comparable to that of other transonic compressor rotors. The use of guide vanes resulted in a circumferential variation in rotor-outlet flow due largely to variations in outlet total pressure when the rotor-tip inlet relative Mach number was greater than 1.0.

## INTRODUCTION

Certain desirable performance characteristics of transonic compressor rotors have been revealed in the investigations of references 1 to 3. These machines did not have inlet guide vanes. This type of rotor design permits the use of free-vortex velocity diagrams with relatively high work inputs and high weight flow at the expense of high blade inlet relative Mach numbers. Such designs are made feasible by the use of certain airfoil shapes (such as the double-circular-arc blade) that perform much better at these high Mach numbers than those shapes most suitable for subsonic machines (such as airfoils having the NACA 65-series thickness distribution).

Because of the relative success of such experimental designs, further studies have been made to determine the value of transonic stages in the

complete engine. One result of such studies is the suggestion that more design freedom might be obtained if a certain amount of whirl were allowed at each rotor inlet. In the first stage of a compressor this prewhirl would, of course, be established by inlet guide vanes. The use of these guide vanes would not necessarily be for the purpose of reducing the rotor blade inlet relative Mach numbers, but perhaps to satisfy some other design condition.

In considering the design of such an inlet stage, it must first be assumed that the effect of one blade row on the other will be negligible. If this assumption were not made, it would be difficult to find any design data. Experience has shown that this assumption is a sufficiently valid one if the design of a subsonic stage is required. No such experience has been accumulated, however, for a transonic stage. The principal purpose of this investigation was to determine whether or not there exist any blade-row interactions of sufficient magnitude to affect rotor performance of a transonic inlet stage.

To accomplish this purpose, a compressor rotor utilizing inlet guide vanes was designed and built. The purpose of the inlet guide vanes was to establish a velocity diagram that would reduce rotor-tip diffusion factors below those usually encountered at the desired work input. To evaluate the effects of blade-row interaction, both circumferential and radial variations of the flow conditions were measured at the rotor inlet and outlet. The experimental results of this investigation are presented in the form of over-all performance, blade-element performance, and circumferential variations in blade-element performance.

## SYMBOLS

$A_F$    compressor frontal area based on rotor-tip diameter, sq ft

$D$     diffusion factor (ref. 10)

$g$     acceleration due to gravity, 32.174 ft/sec$^2$

$H$     total specific enthalpy

$i$     incidence angle, angle between inlet-air direction and tangent to blade mean camber line at leading edge, deg

$M$     Mach number

$n$     number of blades

$P$     total pressure, lb/sq ft or in. Hg

p       static pressure, lb/sq ft

r       radius measured from axis of rotation, ft or in.

$r_c$       radius of curvature

T       total temperature, $^\circ$R

U       blade speed, ft/sec

V       air velocity, ft/sec

w       weight flow of air, lb/sec

$\beta$       air angle, angle between air velocity and axial direction, deg

$\gamma^\circ$       blade-chord angle, angle between blade chord and axial direction, deg

$\delta$       ratio of inlet total pressure to NACA standard sea-level pressure of 2116 lb/sq ft

$\delta^\circ$       deviation angle, angle between outlet-air direction and tangent to blade mean camber line at trailing edge, deg

$\eta$       adiabatic temperature-rise efficiency

$\theta$       ratio of inlet total temperature to NACA standard sea-level temperature of 518.7$^\circ$ R

$\rho$       static density of air, lb/cu ft

$\sigma$       solidity, ratio of blade chord measured along streamline to average blade spacing

$\varphi$       blade camber angle, difference between angles of tangents to mean camber line at leading and trailing edges, deg

$\bar{\omega}$       total-pressure-loss coefficient

Subscripts:

h       hub

m       midradius survey position

m.a.       mass-averaged value

t        tip

z        axial direction

$\theta$        tangential direction

0        depression tank

1        upstream of guide vane

2        between guide vane and rotor

3        rotor outlet

Superscript:

'        relative to rotor


### COMPRESSOR DESIGN

#### Rotor

The rotor of this investigation, shown in figure 1, was designed to have the following characteristics:

Total-pressure ratio, $P_3/P_2$ . . . . . . . . . . . . . . . . . . . . 1.35
Adiabatic efficiency, $\eta$ . . . . . . . . . . . . . . . . . . . . . . 0.90
Tip speed, $U_t$, ft/sec . . . . . . . . . . . . . . . . . . . . . . 1000
Equivalent weight flow per square foot of frontal area, $w\sqrt{\theta}/\delta A_F$,
   (lb/sec)/sq ft . . . . . . . . . . . . . . . . . . . . . . . 31.5
Inlet hub-tip radius ratio, $r_h/r_t$ . . . . . . . . . . . . . . . . . 0.5
Number of blades, n . . . . . . . . . . . . . . . . . . . . . . . . 34
Tip solidity, $\sigma_t$ . . . . . . . . . . . . . . . . . . . . . . . 1.0
Tip radius, $r_t$, ft . . . . . . . . . . . . . . . . . . . . . . . 0.75
Tip axial velocity ratio, $(V_{z,3}/V_{z,2})_t$ . . . . . . . . . . . . . . 1.0

The values of chord length, pressure ratio, and efficiency were assigned as constant with radius in the design calculations. The velocity diagrams at both inlet and outlet were then established by specifying the rotor-inlet absolute flow angles and by requiring that the simple-radial-equilibrium equation

$$\frac{dp}{dr} = \frac{\rho}{g}\frac{V_\theta^2}{r} \tag{1}$$

and flow continuity be established at both the rotor-inlet and -outlet stations.

Several different distributions of inlet flow angle were prescribed, and the resulting designs were compared and studied. From this study the final design variation of rotor-inlet absolute flow angle was chosen. This was a linear variation with radius of $-14^O$ at the tip to $-3^O$ at the hub. The principal reason for this choice was that it resulted in a compromise between rotor blade relative inlet Mach number and rotor blade diffusion factor that was believed most suitable.

A rotor-outlet blockage factor of 0.96 was specified, and the outlet hub-tip radius ratio, consistent with flow continuity, was found to be 0.589. The blade shape was selected as double circular arc in the cylindrical (r = const.) surface. The incidence angles were set at a radially constant value of $4^O$ based upon reference 1, and the deviation angles were obtained from Carter's rule (ref. 4). More recent data of reference 5 (ch. VII) show that this design incidence angle assumption is poor, but the deviation-angle rule is good.

## Guide Vanes

In order to obtain the desired inlet tangential velocity distribution, a set of guide-vane blades was designed for a turning of $14^O$ at the rotor tip and $3^O$ at the rotor hub counter to the direction of rotor whirl, with a linear variation from hub to tip. The effects of secondary flow on this turning distribution were computed by the method of reference 6. The turning angles were modified according to the results of these computations. The blade profile was selected from reference 7, since the 63-series blade shape indicated low losses for a relatively high inlet Mach number. The carpet plots of reference 7 were used for a constant solidity of 0.75. The blade profile was determined at four equally spaced radial stations. The blade geometry is presented in table I.

## INSTALLATION AND INSTRUMENTATION

The variable-component test rig described in reference 2 was modified for the installation of rotor and guide vanes. A schematic sketch of the installation is given in figure 2.

The instrumentation of reference 2 was used with the addition of a survey station located approximately 0.25 inch behind the guide-vane tips. The locations of the survey stations are indicated in figure 2. In addition to this instrumentation, a circumferential pad located 0.25 inch behind the rotor and at an angle equal to the taper of the blade trailing edge was available for conducting circumferential surveys at any desired radius with either a combination survey probe or a hot-wire-anemometer probe. The circumferential survey instruments are shown in figure 3(a) with a survey probe installed in the casing mounting.

The guide-vane performance was obtained at ten radial stations by the use of a circumferential total-pressure rake, a miniature L-static probe, and a total-pressure claw probe. The rotor exit was surveyed at ten radial stations with two sting-mounted wedge static probes and three combination survey probes. The radial survey instruments are shown in figure 3(b). All temperature and static-pressure probes were calibrated for Mach number and density effects. A magnetic-type vibration pickup mounted a short distance upstream of the rotor was used to detect the blade vibration.

The circumferential variations observed in this investigation raise some doubt as to the validity of the blade-element data. The main concern was whether or not the three survey instruments used to measure rotor-outlet absolute flow angle, total pressure, and total temperature gave average flow data from which an accurate representation of the rotor performance could be obtained. A detailed study of the problem revealed that the data presented are probably as accurate as other blade-element data available at this time.

## PROCEDURE

The rotor was investigated over a range of weight flows at corrected tip speeds of 700, 800, 900, and 1000 feet per second (70, 80, 90, and 100 percent of design speed). Maximum weight flow was limited by the rotor. The minimum weight flow was determined by rotor blade vibrations or by compressor surge. The inlet depression-tank pressure was held at 20 inches of mercury absolute. Over-all rotor performance was obtained by mass-averaging the blade-element performance at station 3 as shown in reference 8.

## RESULTS AND DISCUSSION

### Over-all Performance

The over-all performance characteristics of this compressor rotor are shown in figure 4. At 100-percent design speed, a choke weight flow of approximately 30.5 pounds per second per square foot of frontal area was obtained. The mass-averaged total-pressure ratio reached a maximum at 1.40. At design speed a peak abiabatic efficiency of 0.89 was obtained at a weight flow of 29.04 pounds per second per square foot and a pressure ratio of 1.39. As the speed was decreased, the peak adiabatic efficiency increased to a maximum value of 0.95 at 80-percent speed. In general, the over-all characteristics of this transonic compressor rotor with inlet guide vanes are similar to those of reference 2, where no inlet guide vanes were used.

## Guide-Vane Performance

The guide vanes used in this investigation were required to do a relatively small amount of turning. For this reason, the performance of this blade row is of interest only to establish the rotor-inlet flow conditions.

Surveys of the radial variation of absolute flow angle leaving the guide vanes were made for several mass-flow rates. The results of these surveys are shown in figure 5, where the average measured variation is indicated by the solid line. This average variation was assumed in all later tests.

The radial variation of guide-vane total-pressure loss was also measured for several mass-flow rates. A 23-tube circumferential wake rake was used to obtain the total-pressure loss of one of the guide vanes. The wake pressure loss for each radial station was arithmetically averaged over one guide-vane passage, and these average values were converted to a total-pressure-loss coefficient. These total-pressure-loss coefficients are plotted against radius ratio for several equivalent weight flows in figure 6(a). The losses in the inlet guide vanes are relatively small, becoming significant only at the tip and hub regions. In all later tests, the total pressure at the rotor inlet was determined by means of these data and the measured inlet-tank total pressure.

A typical loss distribution in the blade-wake region is illustrated in figure 6(b). The guide-vane wake is relatively narrow and reaches a maximum loss coefficient of about 0.28. Thus, the wake of the guide vane passing into the compressor rotor appeared to be relatively small.

## Rotor-Inlet Conditions

The radial conditions at the inlet of the compressor rotor are shown in figure 7 for 100, 90, and 80 percent of design speed. Three operating conditions are shown for each speed. These conditions are designated A, B, C, and are indicated on the over-all performance plot of figure 4. Operating condition A refers to the minimum-weight-flow point, condition B to the approximate peak-efficiency point, and condition C to the maximum-weight-flow point.

The design distribution of axial velocity was not achieved in the experimental results. In the tip region experimental axial velocity was somewhat higher than the design value, while in the hub region the axial velocity is sizably lower than the design value. This departure from design is further reflected in the plots of absolute and relative Mach number. Thus, the inlet flow conditions to the rotor were not set up according to the design flow conditions, and particularly the hub could

not be expected to operate at design condition.  Similar variations in
flow condition can be observed at 90- and 80-percent speed.

## Rotor-Outlet Conditions

Rotor-outlet flow conditions are shown in figure 8 for the same
speeds and operating conditions as in figure 7.  These values were obtained
from the radial surveys of three combination probes and two wedge static
probes.  The largest variation in total-pressure ratio is obtained in
the tip region.  This characteristic is similar to that observed in other
compressor rotors and is partly a function of the vector diagram.  For
the peak-efficiency operating condition B at design speed, the pressure
ratio is higher than the design value of 1.35 (fig. 8(a)).  The measured
adiabatic efficiency for the peak-efficiency point falls continuously
from hub to tip.  At the peak-efficiency operating point, the other exit
flow conditions do not exhibit design trends except the exit absolute
Mach number.  The exit axial velocity at the peak-efficiency operating
point compares favorably with the design values in the tip region; however,
it departs from design in the hub region, as at the rotor inlet.

Discharge flow conditions at the lower speeds vary essentially the
same as those at design speed.  The pressure ratio at the 80-percent-
speed point for maximum-efficiency operation is essentially constant across
the radius, indicating that the energy addition is essentially constant
along the radius.

## Consideration of Radial Equilibrium

Rotor-inlet conditions. - Three test points were chosen as repre-
sentative of rotor-inlet conditions, two at design speed and the other
at 80-percent design speed.  The design-speed points are B and D of
figure 4, and the 80-percent speed point is point B.  Figure 9(a) is a
plot of the radial variation of $V_{z,2}/V_{z,2,m}$ of the experimental data
and the curve computed by the simplified-radial-equilibrium equation (1),
which is derived in reference 9.  For the computation of the simplified-
radial-equilibrium curve, the total pressure, tangential velocity, and
total temperature were taken equal to the experimental data.  The results
of the computations shown in figure 9(a) indicate that the compressor
did not display the flow conditions indicated by the simplified-radial-
equilibrium computations at the rotor inlet.  The large difference at
the rotor hub was caused by wall curvature at the rotor inlet, which is
ignored in this form of the radial-equilibrium equation.

The radial variation of rotor-inlet streamline curvature is plotted
in figure 10(a).  The points on this curve were computed by the use of

Euler's equation of motion in radial direction with the assumptions that the flow was time-steady, there were no fluid forces, the radial component of velocity was zero, and the flow was axisymmetric. These assumptions give the following equation:

$$\frac{1}{\rho}\frac{\partial p}{\partial r} = \frac{V_\theta^2}{r} + \frac{V_z^2}{r_\mathscr{C}} \qquad (2)$$

The difference between this equation and the simplified-radial-equilibrium equation is the curvature term $V_z/r_\mathscr{C}$. The radial variation of $1/r_\mathscr{C}$ was computed from equation (2) and experimental data, and the wall values of curvature are included to show their agreement with the computed streamline curvature. This computation shows that the wall curvature is an important design criterion for high-mass-flow compressors.

Rotor-outlet conditions. - The same three points used in the inlet computations were computed for simplified radial equilibrium and streamline curvature at the rotor outlet. Figure 9(b) illustrates the rotor-outlet conditions plotted as a radial variation of $V_{z,3}/V_{z,3,m}$. The measured data at the rotor outlet were used for the computation. With this method the entropy and enthalpy gradients are included in the simplified-radial-equilibrium expression. The difference between the simplified-radial-equilibrium computations and experimental results again is due to streamline curvature.

The results of the computation for outlet streamline curvature are shown in figure 10(b) with the wall values. The wall curvature at the rotor outlet appears to be a factor for the establishment of design conditions for this compressor, but the effect is not as strong as at the inlet.

Blade-Element Performance

To simplify the analysis of this rotor, the streamlines that lie in the r-z plane (containing the axis of rotation and radial line) were assumed to be straight lines dividing the annular passage height into equal-percentage radial increments at the inlet and outlet of the rotor blades. The blade elements referred to in this report are sections of rotor blades that lie in stream surfaces of revolution generated by rotating the assumed streamlines about the axis of rotation.

Blade-element performance of this rotor is presented in figure 11 for four speeds at three blade-element sections. These sections are located at 10, 50, and 90 percent of the passage height from the outer wall and are called tip, mean, and hub blade elements, respectively. The

measured geometries of these sections are tabulated in table II. The
calculations and the significance of the various parameters in rotor
blade-element analysis are discussed in references 8 and 10.

Relative total-pressure-loss coefficient. - The blade-element loss
data shown in figure 11 indicate that, at the hub and mean sections, the
minimum total-pressure-loss coefficient is essentially independent of
rotor speed. At the tip, however, a marked increase in loss is indicated
for the two highest operating speeds. Figure 12 shows the relation of
loss coefficients in the region of minimum loss taken from faired values
of figure 11 and plotted against corresponding faired values of diffusion
factor. The increase in tip-element loss associated with the increase
in rotor speed is accompanied by an increase in diffusion factor. Mach
number effects (shock losses and blade-row interaction) were not present
to a great enough degree to cause losses appreciably beyond the range
of correlation for a number of compressors having subsonic tip-element
operation as presented in reference 11 and reproduced in figure 12.

Deviation angle. - The measured deviation angles at minimum-loss
incidence angle are compared with Carter's rule (ref. 4) and the cascade
rule and deduced variations of reference 5 in figure 13. The deviation
angles are plotted against inlet relative Mach number for comparison
purposes only. All three deviation-angle rules agree well with the ob-
served values for the tip and mean blade elements. For the hub element
it appears that deviation-angle predictions obtained from Carter's rule
agree with observed values somewhat better than those of the other two
rules.


Axial Asymmetry in Rotor-Outlet Flow

Measured variations. - During rotor performance tests at tip speeds
of 900 and 1000 feet per second, large circumferential variations in
rotor-outlet flow conditions were noticed. This condition was confirmed
by use of the circumferential survey instrument described earlier. Fig-
ure 14(a) shows the circumferential variations of measured outlet total
pressure and temperature and blade-element loss for the tip element
during operation at a tip speed of 900 feet per second and an incidence
angle of approximately 4.2° (indicated by the letter E in fig. 11(a)).

The abscissa in this figure is circumferential position in arbitrary
units. The total length of survey is about one guide-vane spacing. It
can be seen from figure 14(a) that the total-pressure-loss coefficient
ranges from about 0.095 to 0.075 over a large part of the circumference.
However, the loss coefficient increases rapidly to a value near 0.20 over
a portion of the circumference. These large variations are due to an
interaction between the rotor and guide-vane rows.

4107

CB-2 back

The variations in the loss coefficient were primarily due to cir-
cumferential variations in rotor-outlet total pressure. These variations
with circumferential position were present only at the outlet of those
blade elements operating at inlet relative Mach numbers greater than 1.0.
Thus, as the rotor tip speed was increased from 900 to 1000 feet per
second, a larger portion of the outlet annulus became involved. This
increase in speed with a corresponding change in minimum-loss incidence
angle to approximately 5.3° for the tip element (corresponding to the
letter F in fig. 11(a)) also resulted in a general rise in the rotor
loss coefficient, as shown in figure 14(b). Except for this magnitude
difference, however, the variations are alike for these two speeds.

A hot-wire anemometer was employed using the procedure reported in
reference 12 for the purpose of studying the rotor-outlet flow in more
detail. The accuracy of the results obtained is somewhat questionable,
because the calculations outlined in reference 12 are less applicable
to the case of a rotor and guide-vane combination. However, the cir-
cumferential averages of the losses measured by this method agree
reasonably well with those of figure 14(a). Figure 15 shows the cir-
cumferential variation of relative total-pressure-loss coefficient for
the tip element at operating point E as obtained by these hot-wire-
anemometer measurements. Several corresponding oscilloscope traces of
the blade wakes from which these values were obtained are shown in order
in figure 16. It may be seen from these two figures that the local high-
loss regions in the rotor-outlet annulus are regions into which an
abnormally large blade wake is shed by the passing rotor blades.

Effect of guide-vane wakes on vector diagram. - It has already been
mentioned that circumferential variations in the rotor-outlet flow were
observed whenever the inlet relative Mach number was greater than 1.0.
This relation is probably not a mere coincidence. On the other hand,
previous investigations show that no sudden changes occur in the per-
formance of a blade element as the inlet relative Mach number passes
through 1.0.

It is important to point out that the large circumferential variations
in outlet flow conditions could not have been predicted by consideration
of vector diagrams. This method of analysis is used to determine quali-
tatively the development of blade wakes as they pass through a succeeding
blade row. A vector-diagram analysis requires some assumptions of rotor
performance such as the variations of total-pressure-loss coefficient with
incidence angle. In the present investigation, such an analysis would
have failed to predict the observed correlation between rotor-inlet rela-
tive Mach number and the magnitude of the rotor-outlet circumferential
variations. As an example, a calculation based upon guide-vane-wake
measurements and rotor performance data from a typical design-speed test
point gave the following results:

(1) If the guide-vane wake underwent little or no diffusion beyond the point at which it was measured (3/8 in. downstream of blade trailing edge), a variation of about $2^\circ$ in rotor blade incidence angle would have resulted each time these blades passed through a guide-vane wake.

(2) This $2^\circ$ variation in incidence angle from point F of figure 11(a) would have resulted in a change in loss coefficient from about 0.125 to 0.140.

The measured loss variations, however, were greater than those predicted by almost a factor of 10. Furthermore, there is good reason to believe that the guide-vane wakes actually underwent considerably more diffusion before reaching the rotor blades, which would have resulted in a much smaller variation in rotor incidence angle than the $2^\circ$ value referred to. The circumferential variations measured in the rotor-outlet flow were very small whenever the corresponding inlet relative Mach number for that particular survey station was below 1.0. These small variations are in better agreement with the order of magnitude predicted by the vector-diagram analysis.

It is not known whether the phenomenon of axial asymmetry, as observed in this investigation, is present in other transonic machines having two or more blade rows. The authors are unaware of any other published data in which rotor-outlet circumferential surveys were made on a transonic rotor preceded by either guide vanes or stators. As was pointed out in the discussion of the rotor blade-element data, the average loss coefficient for the tip element of this rotor did not appear to be markedly different from that observed in other machines having comparable diffusion factors. In view of this result, it may be concluded that the principal problem of incorporating this type of stage in a multistage compressor is that of determining the effects of the asymmetric rotor-outlet flow on succeeding blade rows. More specifically, the question is whether such a flow will cause the succeeding blade-row performance to differ much from that predicted by the (steady-flow) blade-element or cascade data employed in the design.

## SUMMARY OF RESULTS

The following results were obtained in an experimental investigation of a transonic compressor rotor utilizing inlet guide vanes:

1. Over-all pressure ratio and efficiency of this transonic compressor rotor with inlet guide vanes were comparable to those obtained in other transonic compressor rotors.

2. Measured guide-vane losses were relatively low, and turning angles were very close to the design values.

3. The effect of the guide-vane wakes was to increase the rotor blade-element loss coefficient at relative Mach numbers greater than 1.0 to a value twice that obtained in the region between the guide-vane wakes. The magnitudes of the loss-coefficient variation and the region affected increase with speed. In spite of this circumferential variation of loss coefficient, the average element loss is comparable to that obtained with similar loadings in other investigations.

4. The design radial distributions of axial velocity were not established at the inlet and outlet of this compressor rotor, probably because of the effect of wall curvatures.

Lewis Flight Propulsion Laboratory
    National Advisory Committee for Aeronautics
        Cleveland, Ohio, February 21, 1957

## REFERENCES

1. Lieblein, Seymour, Lewis, George W., Jr., and Sandercock, Donald M.: Experimental Investigation of an Axial-Flow Compressor Inlet Stage Operating at Transonic Relative Inlet Mach Numbers. I - Over-All Performance of Stage with Transonic Rotor and Subsonic Stators up to Rotor Relative Inlet Mach Number of 1.1. NACA RM E52A24, 1952.

2. Tysl, Edward R., Schwenk, Francis C., and Watkins, Thomas B.: Experimental Investigation of a Transonic Compressor Rotor with a 1.5-Inch Chord Length and an Aspect Ratio of 3.0. I - Design, Over-All Performance, and Rotating-Stall Characteristics. NACA RM E54L31, 1955.

3. Robbins, William H., and Glaser, Frederick W.: Investigation of an Axial-Flow-Compressor Rotor with Circular-Arc Blades Operating up to a Rotor-Inlet Relative Mach Number of 1.22. NACA RM E53D24, 1953.

4. Carter, A. D. S.: The Low Speed Performance of Related Aerofoils in Cascade. Rep. No. R.55, British NGTE, Sept. 1949.

5. Members of the Compressor and Turbine Research Division: Aerodynamic Design of Axial-Flow Compressors. Vol. II. NACA RM E56B03a, 1956.

6. Lieblein, Seymour, and Ackley, Richard H.: Secondary Flows in Annular Cascades and Effects on Flow in Inlet Guide Vanes. NACA RM E51G27, 1951.

4107

7. Dunavant, James C.:  Cascade Investigation of Related Series of 6-Percent-Thick Guide-Vane Profiles and Design Charts.  NACA RM L54I02, 1954.

8. Schwenk, Francis C., Lieblein, Seymour, and Lewis, George W., Jr.: Experimental Investigation of an Axial-Flow Compressor Inlet Stage Operating at Transonic Relative Inlet Mach Numbers.  III - Blade-Row Performance of Stage with Transonic Rotor and Subsonic Stator at Corrected Tip Speeds of 800 and 1000 Feet Per Second.  NACA RM E53G17, 1953.

9. Hatch, James E., Giamati, Charles C., and Jackson, Robert J.:  Application of Radial-Equilibrium Condition to Axial-Flow Turbomachine Design Including Consideration of Change of Entropy with Radius Downstream of Blade Row.  NACA RM E54A20, 1954.

10. Lieblein, Seymour:  Review of High-Performance Axial-Flow-Compressor Blade-Element Theory.  NACA RM E53L22, 1954.

11. Lieblein, Seymour, Schwenk, Francis C., and Broderick, Robert L.: Diffusion Factor for Estimating Losses and Limiting Blade Loadings in Axial-Flow-Compressor Blade Elements.  NACA RM E53D01, 1953.

12. Fessler, Theodore E., and Hartmann, Melvin J.:  Preliminary Survey of Compressor Rotor-Blade Wakes and Other Flow Phenomena with a Hot-Wire Anemometer.  NACA RM E56A13, 1956.

4107

TABLE I. - BLADE GEOMETRY OF GUIDE-VANE BLADE

ELEMENTS WITH CONSTANT SOLIDITY OF 0.75

|  | Blade-element radius, r, in. | | | |
|---|---|---|---|---|
|  | 9.000 | 7.438 | 5.875 | 4.312 |
| Chord angle, $\gamma^0$, deg | 12 | 7.48 | 3.95 | 0.60 |
| Camber angle, $\varphi$, deg | 17.4 | 11 | 6.4 | 1.6 |
| Chord length, in. | 1.844 | 1.524 | 1.204 | 0.884 |
| Lift coefficient | 1.125 | 0.695 | 0.395 | 0.110 |
| Leading-edge rad., in. | 0.006 | 0.005 | 0.004 | 0.003 |
| Trailing-edge rad., in. | 0.011 | 0.009 | 0.007 | 0.005 |

TABLE II. - MEASURED ROTOR BLADE GEOMETRIES

OF TIP, MEAN, AND HUB ELEMENTS

|  | Blade element | | |
|---|---|---|---|
|  | Tip | Mean | Hub |
| Camber angle, $\varphi$, deg | 4.7 | 9.8 | 19.6 |
| Chord angle, $\gamma^0$, deg | 51.8 | 41.4 | 23.6 |
| Solidity, $\sigma$ | 1.04 | 1.36 | 1.93 |
| Chord length, in. | 1.67 | 1.72 | 1.84 |
| $\dfrac{\text{Maximum thickness}}{\text{Chord length}}$ | 0.053 | 0.065 | 0.074 |
| Leading- and trailing-edge radii of curvature, $r_{\mathscr{C}}$ | 0.0125 | 0.0125 | 0.0125 |
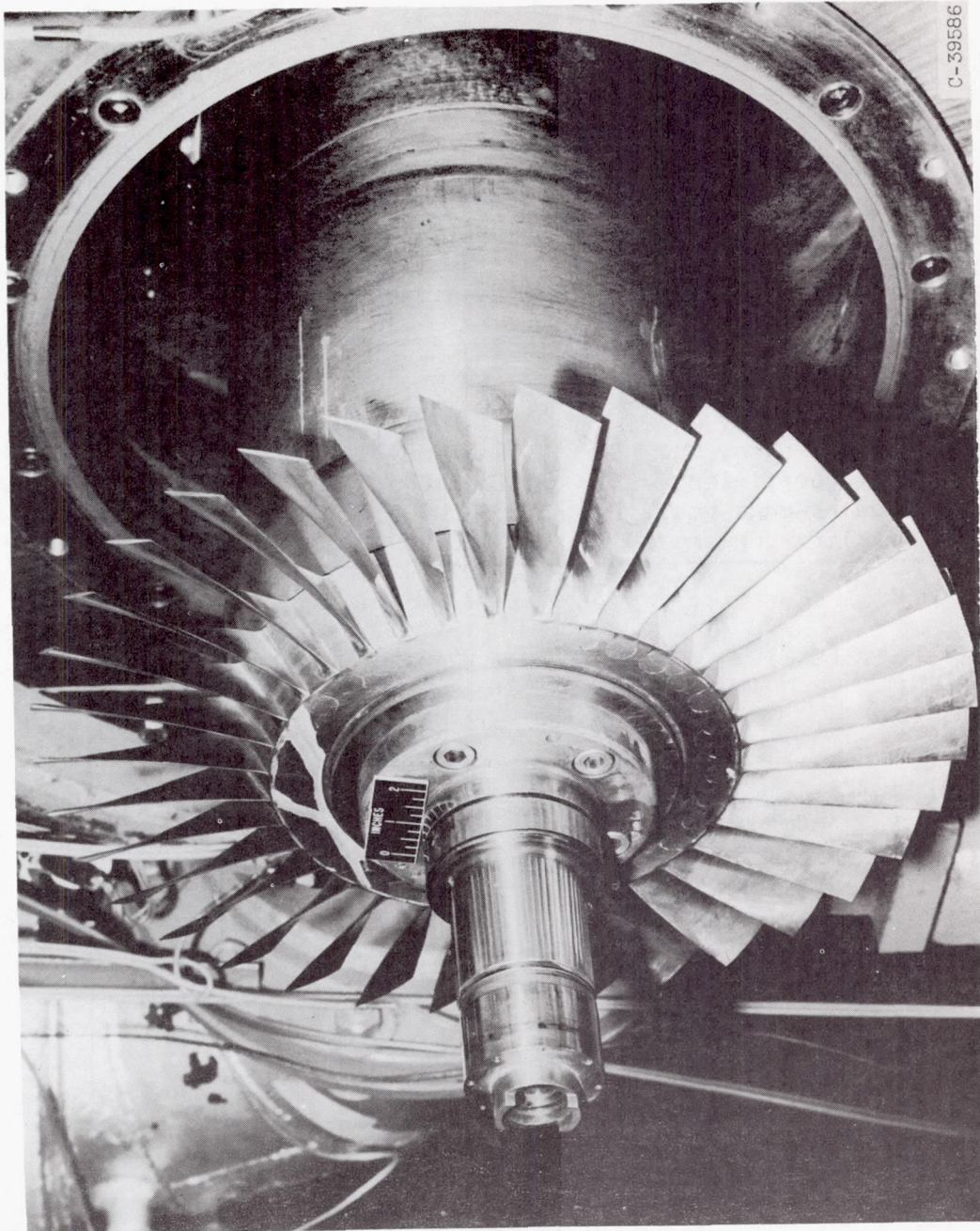
Figure 1. - Photograph of compressor rotor in variable-component test rig.
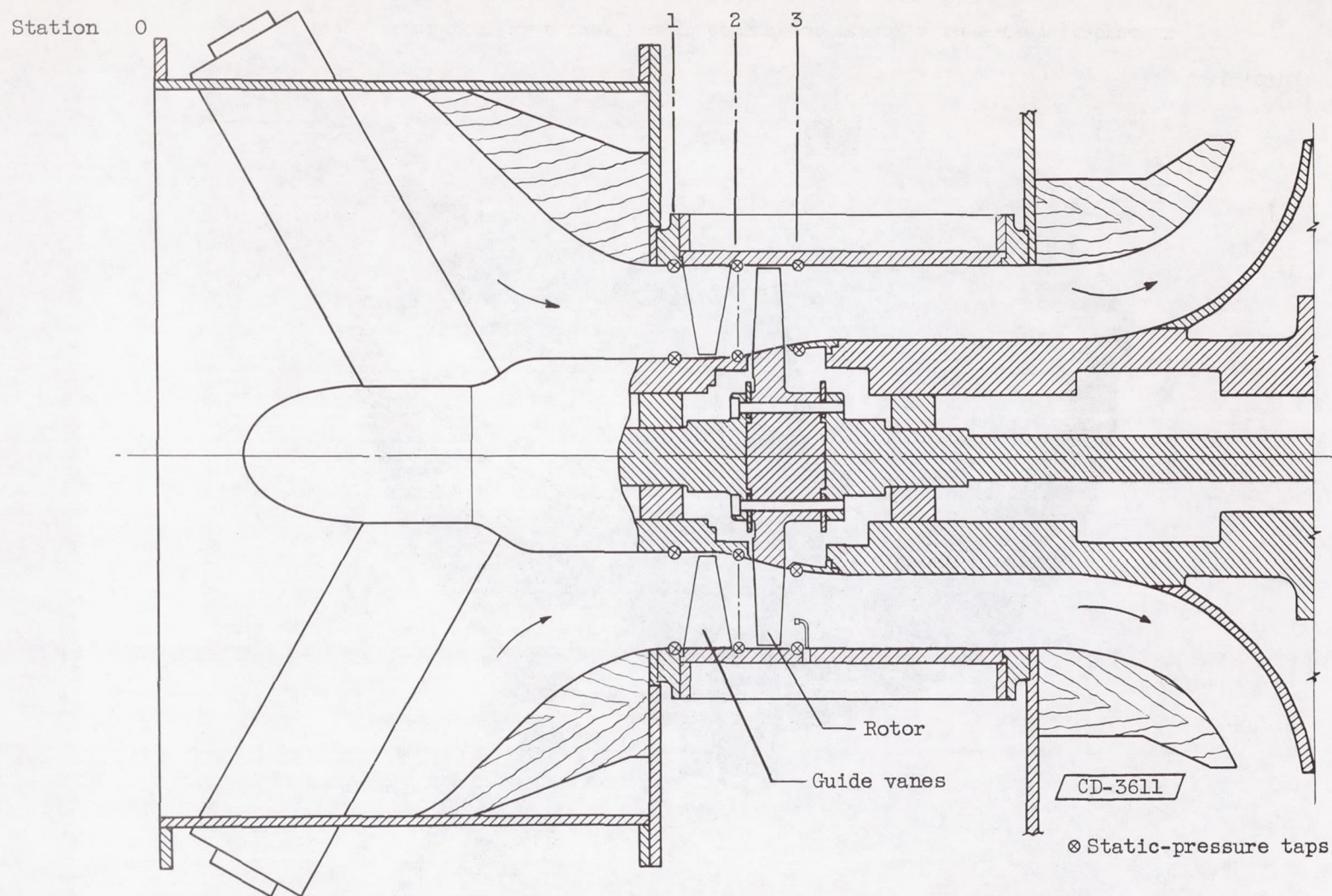
Figure 2. - Schematic sketch of rotor installed in variable-component test rig.

C-42845
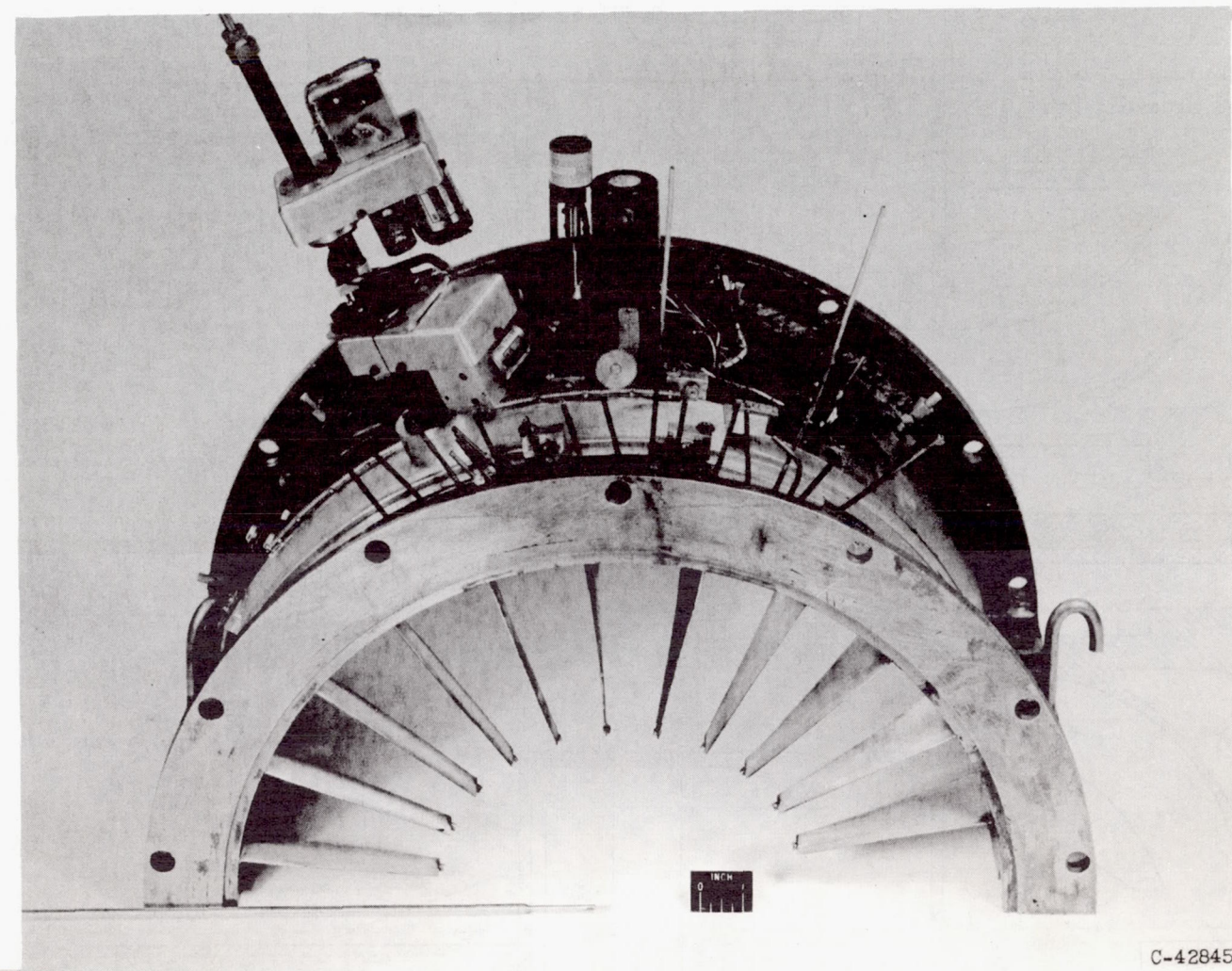
(a) Circumferential survey pad in compressor casing with survey instrument.

Figure 3. - Instrumentation.

L-static probe    Static wedge    Combination probe    Total-pressure claw probe    Total-pressure rake

INCH

0

C-42807
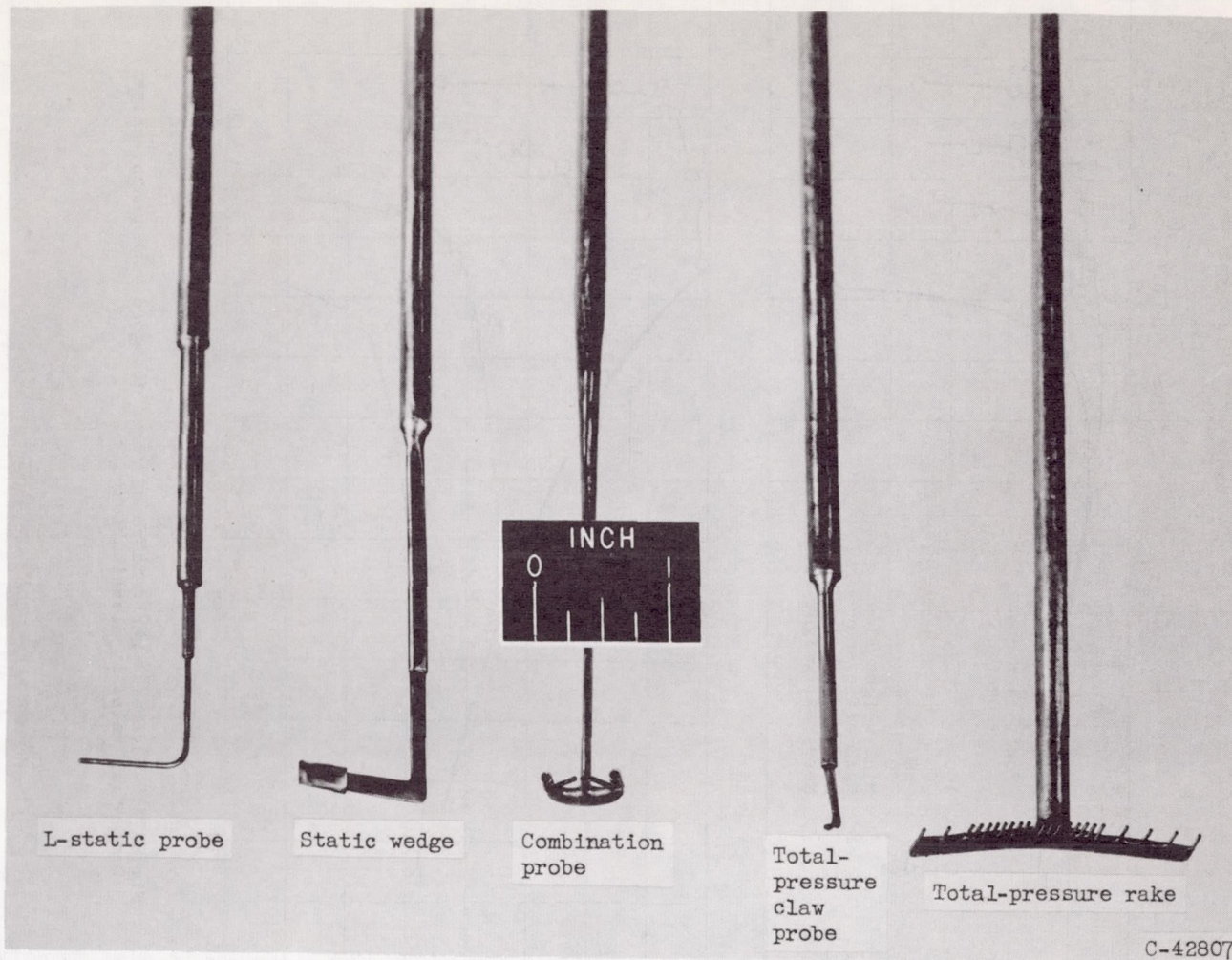
(b) Radial survey instruments.

Figure 3. - Concluded.  Instrumentation.
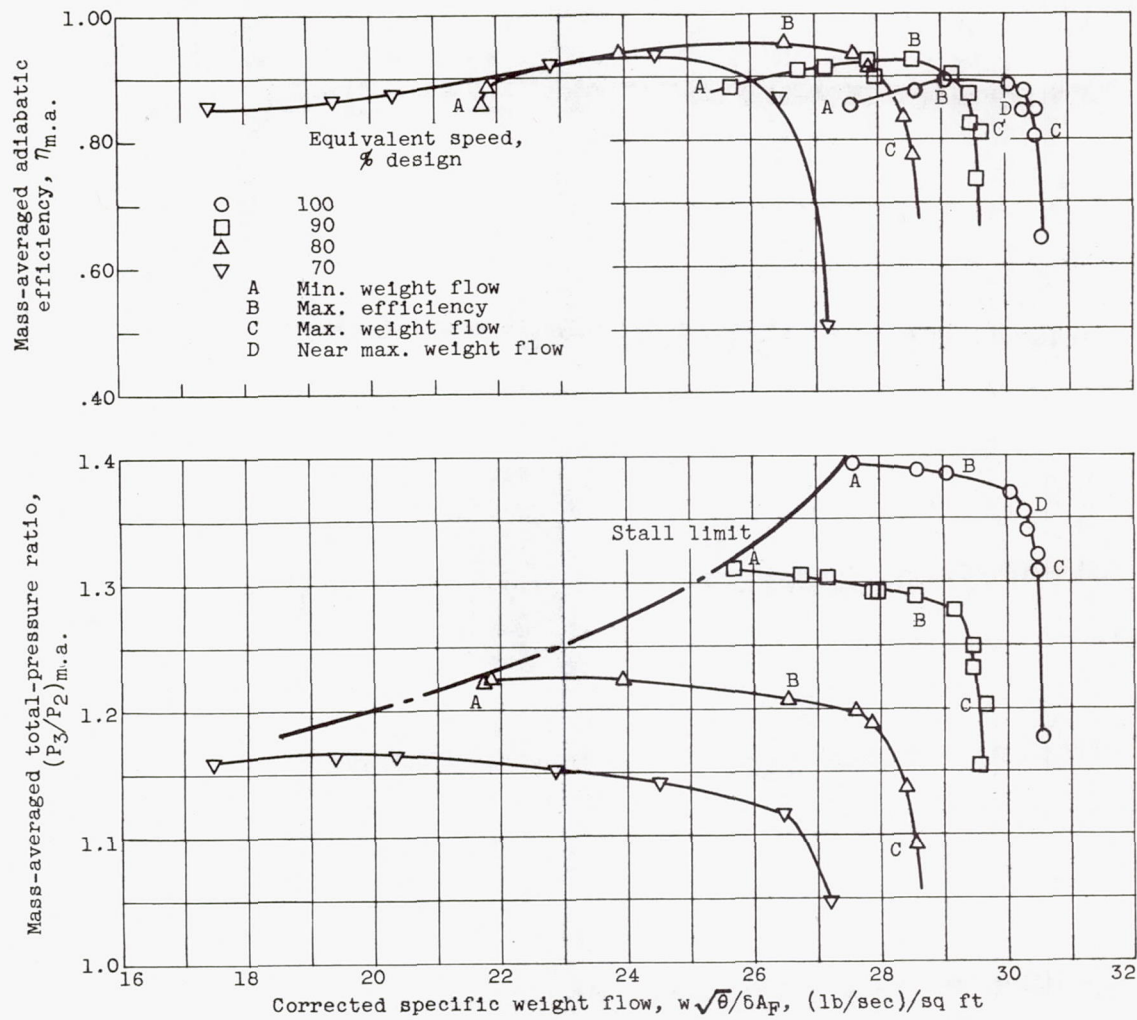
Figure 4. - Over-all performance of rotor designed with unconventional tangential velocity distribution.

4107
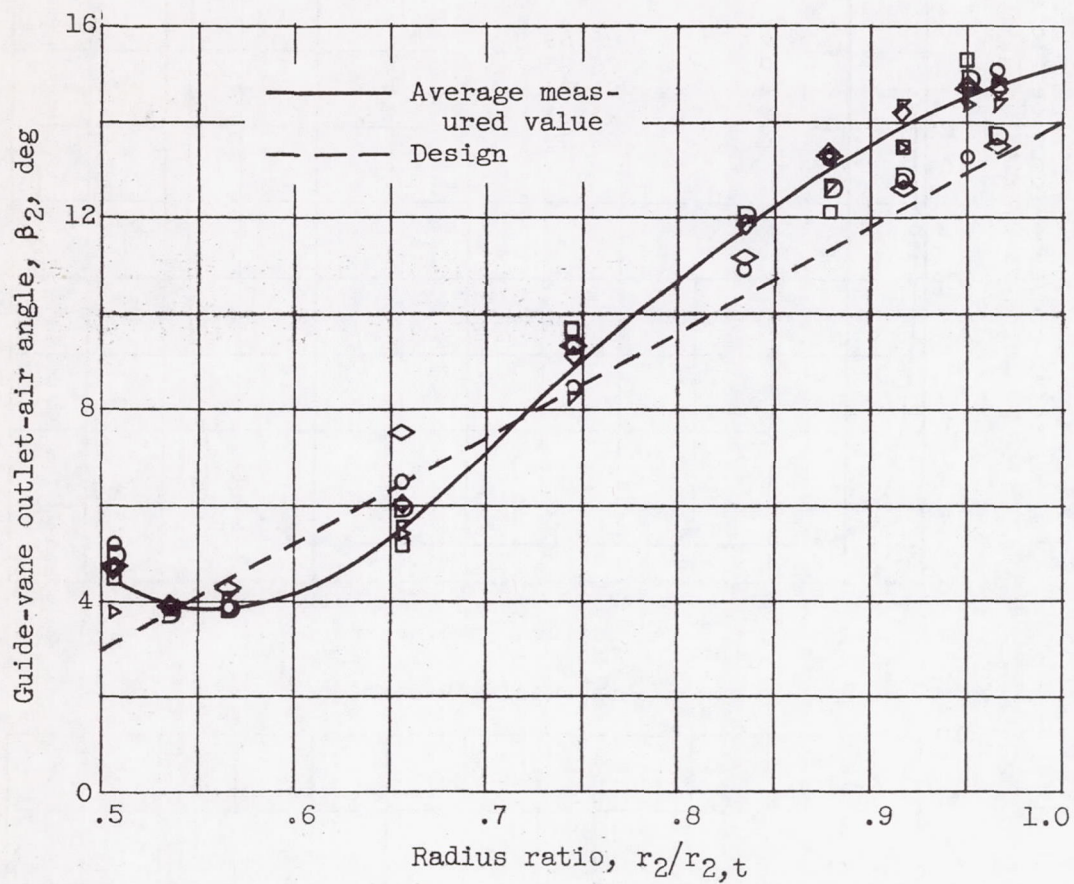


Figure 5. - Experimental guide-vane turning angle.

(a) Radial variation.

(b) Circumferential variation of typical loss profile.
Radius ratio, 0.744.
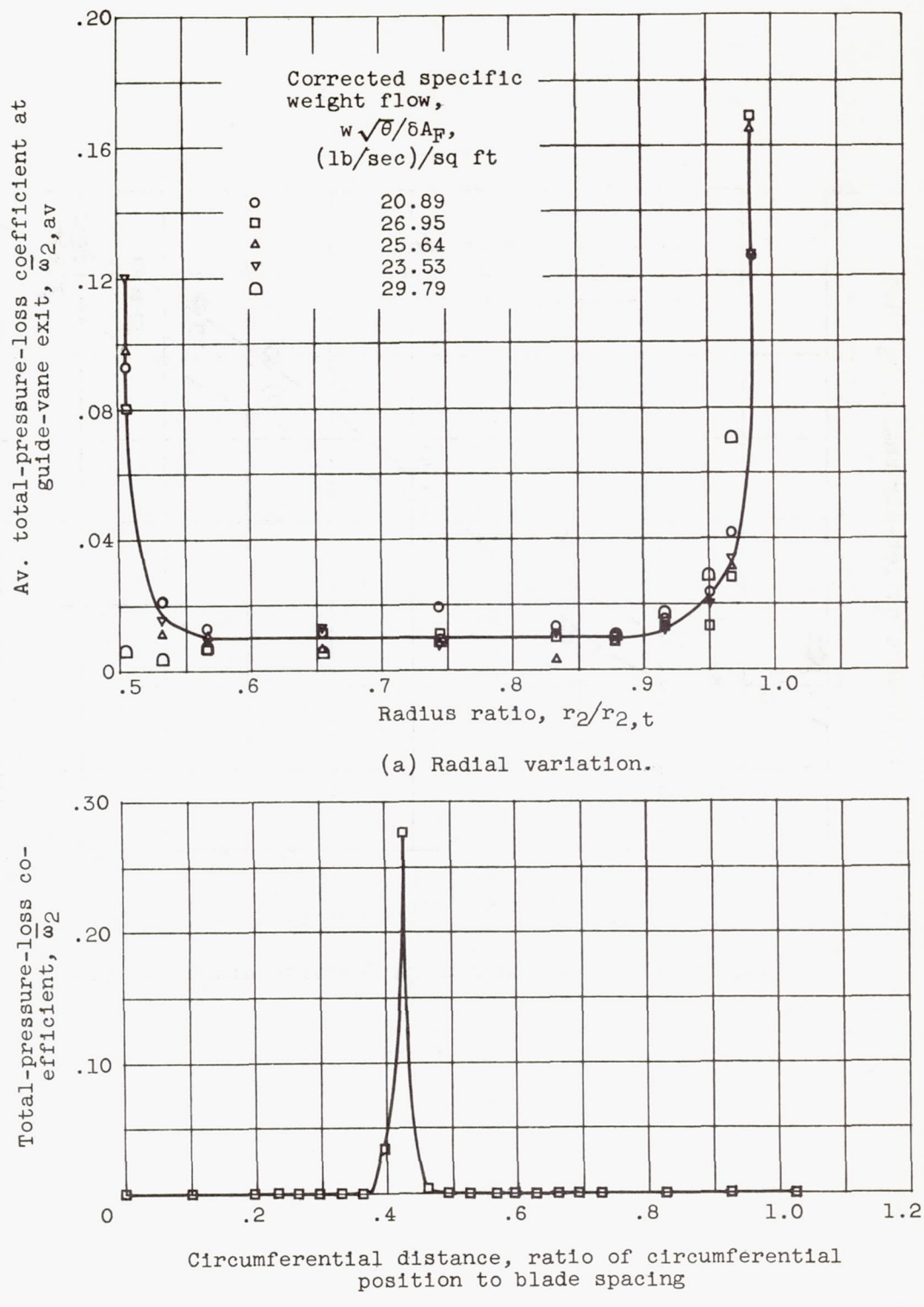
Figure 6. - Guide-vane total-pressure-loss variation.

4107
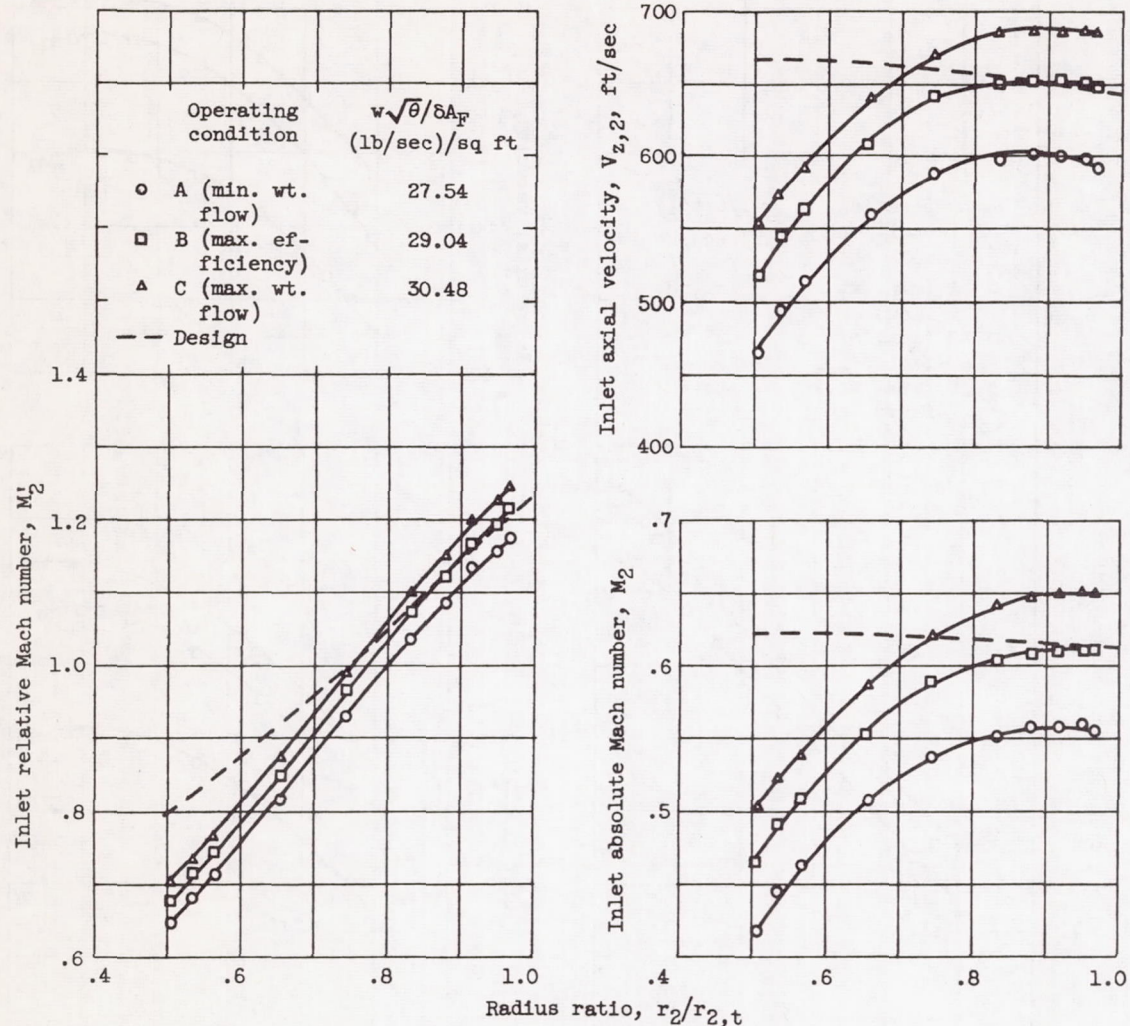


(a) Equivalent speed, 100-percent design.

Figure 7. - Inlet conditions for rotor designed with unconventional tangential velocity distribution.

| Operating condition | $w\sqrt{\theta}/\delta A_F$, (lb/sec)/sq ft |
|---|---|
| ○ A (min. wt. flow) | 25.68 |
| □ B (max. efficiency) | 28.52 |
| △ C (max. wt. flow) | 29.62 |
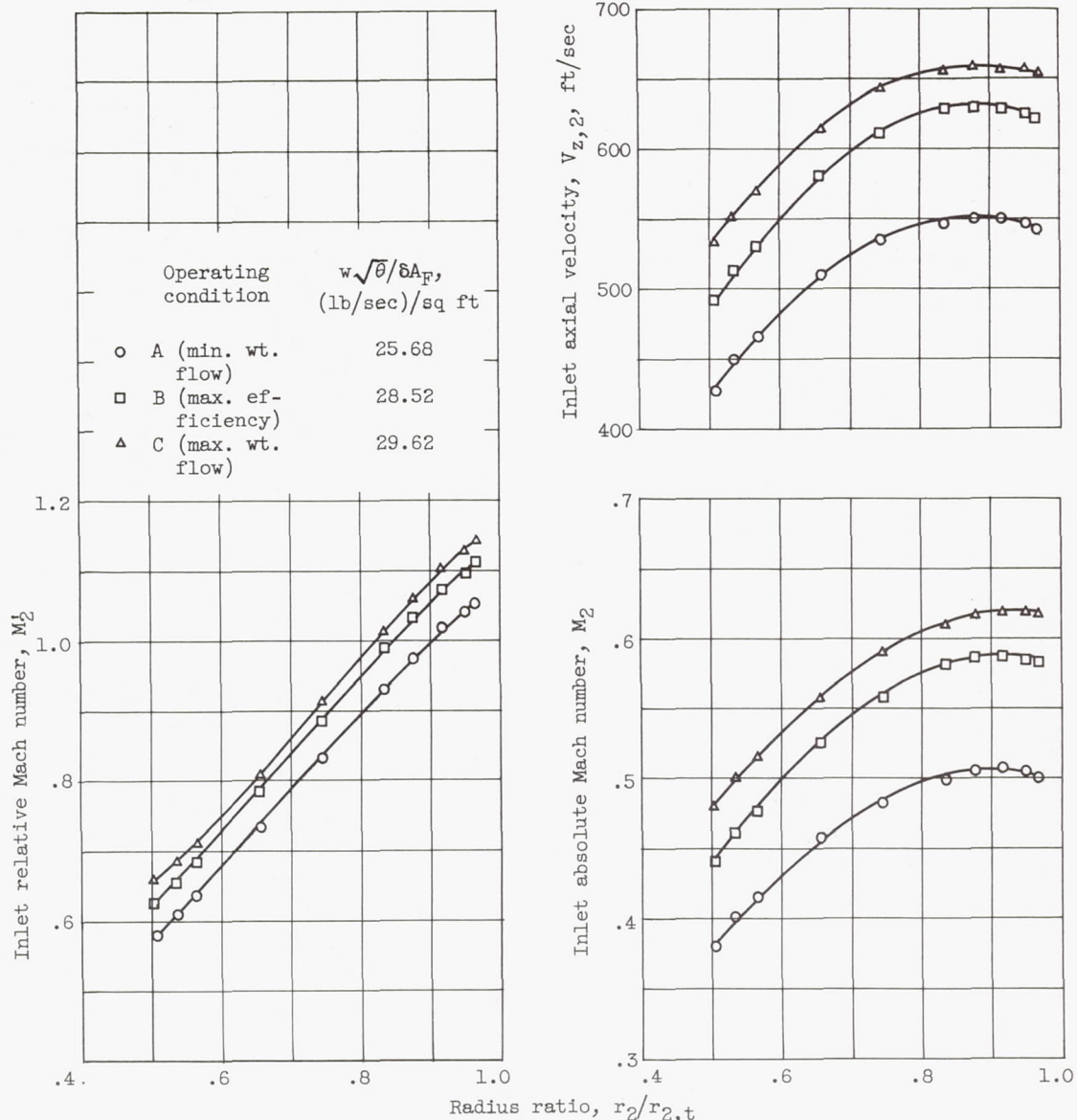
(b) Equivalent speed, 90-percent design.

Figure 7. - Continued.  Inlet conditions for rotor designed with unconventional tangential velocity distribution.

Operating
condition

$w\sqrt{\theta}/\delta A_F$,
$\dfrac{\text{lb/sec}}{\text{sq ft}}$

○  A (min. wt.
      flow)          21.74

□  B (max. ef-
      ficiency)      26.51

△  C (max. wt.
      flow)          28.54

Inlet axial velocity, $V_{z,2}$, ft/sec

Inlet relative Mach number, $M_2'$

Inlet absolute Mach number, $M_2$

Radius ratio, $r_2/r_{2,t}$
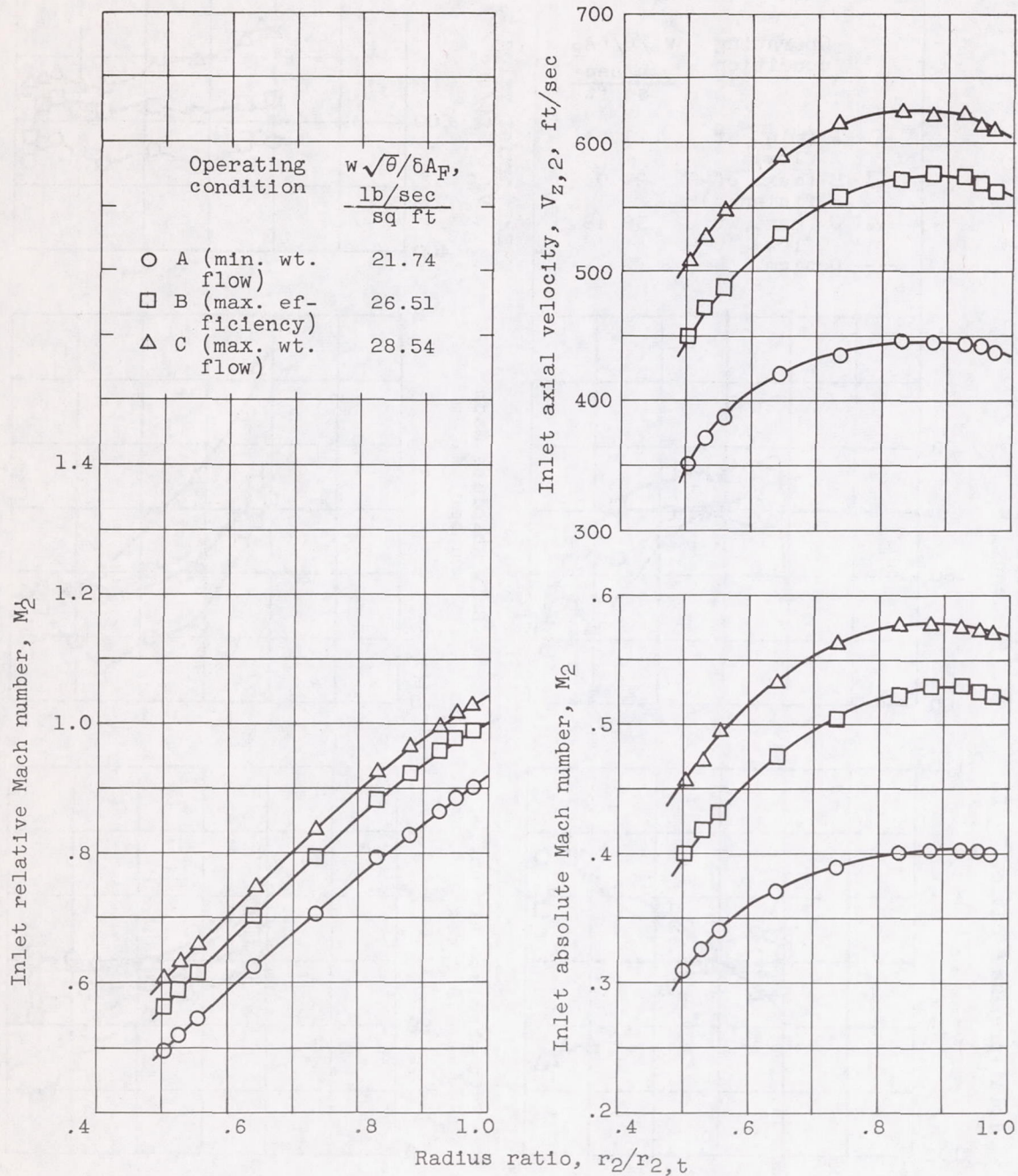
(c) Equivalent speed, 80-percent design.

Figure 7. - Concluded.  Inlet conditions for rotor designed with
unconventional tangential velocity distribution.
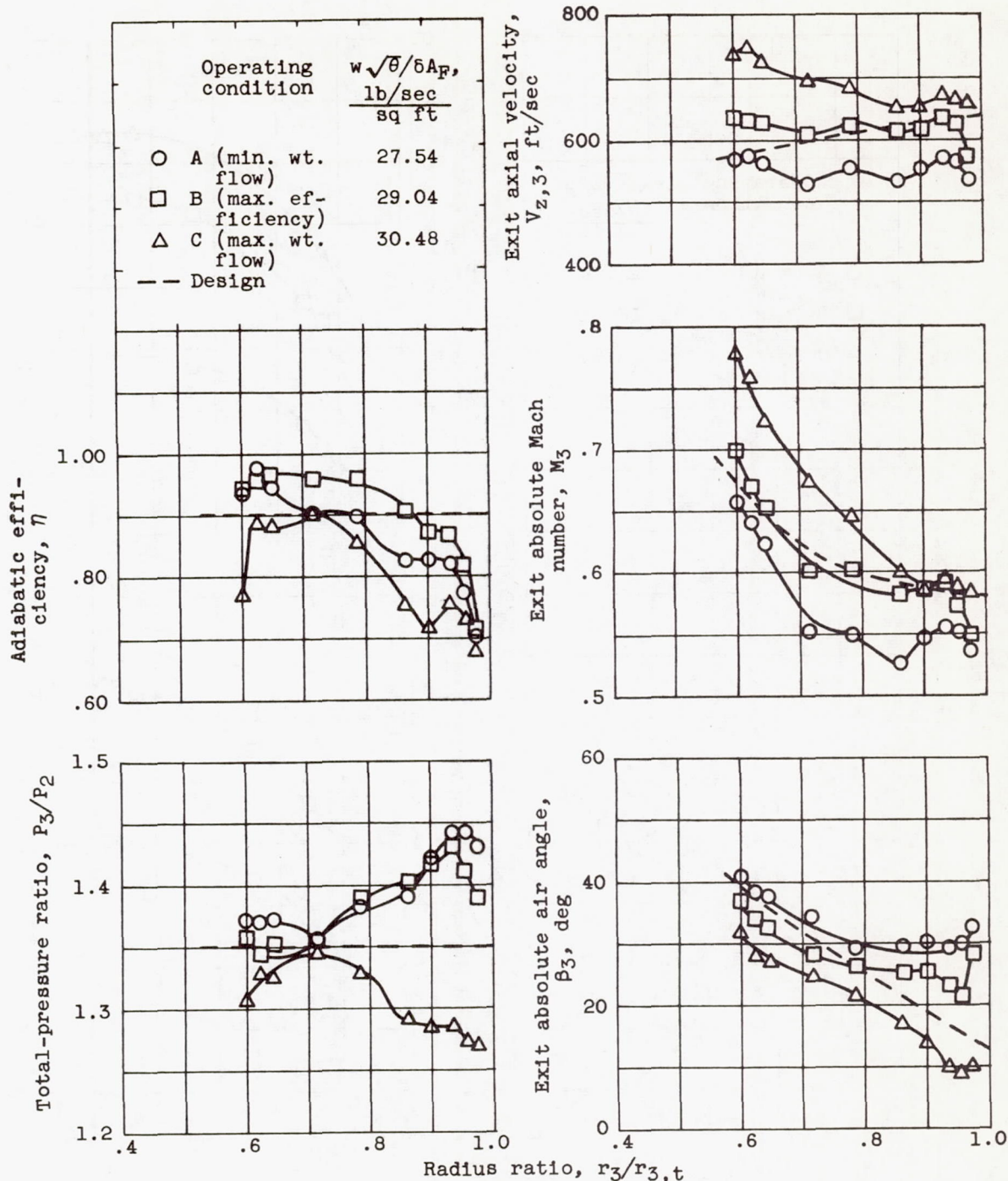
(a) Equivalent speed, 100-percent design.

Figure 8. - Outlet conditions for rotor designed with unconventional tangential velocity distribution.

CB-4 back

4107



| Operating condition | $w\sqrt{\theta}/\delta A_F$, lb/sec sq ft |
|---|---|
| ○ A (min. wt. flow) | 25.68 |
| □ B (max. efficiency) | 28.52 |
| △ C (max. wt. flow) | 29.62 |
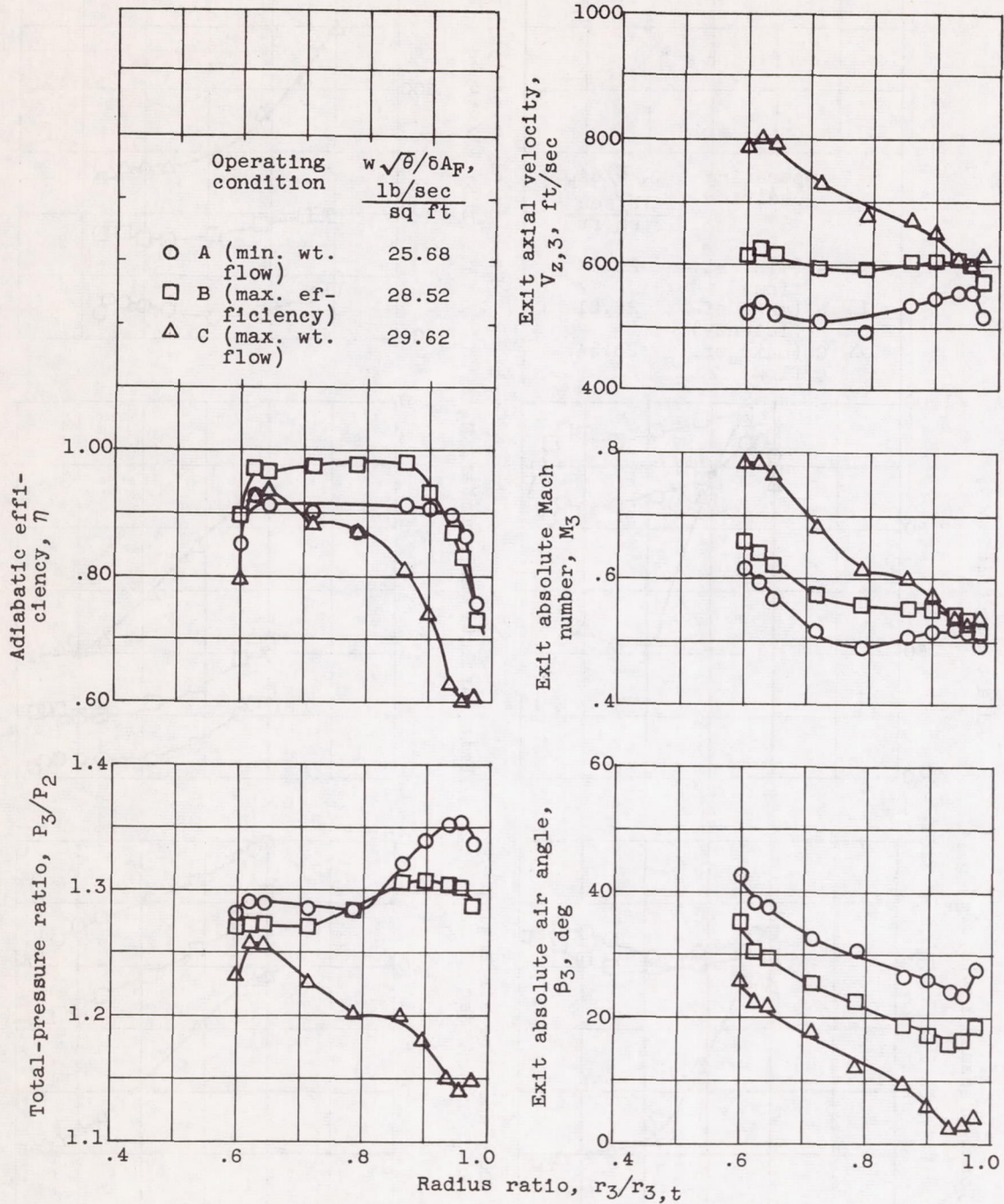
(b) Equivalent speed, 90-percent design.

Figure 8. - Continued.  Outlet conditions for rotor designed with unconventional tangential velocity distribution.
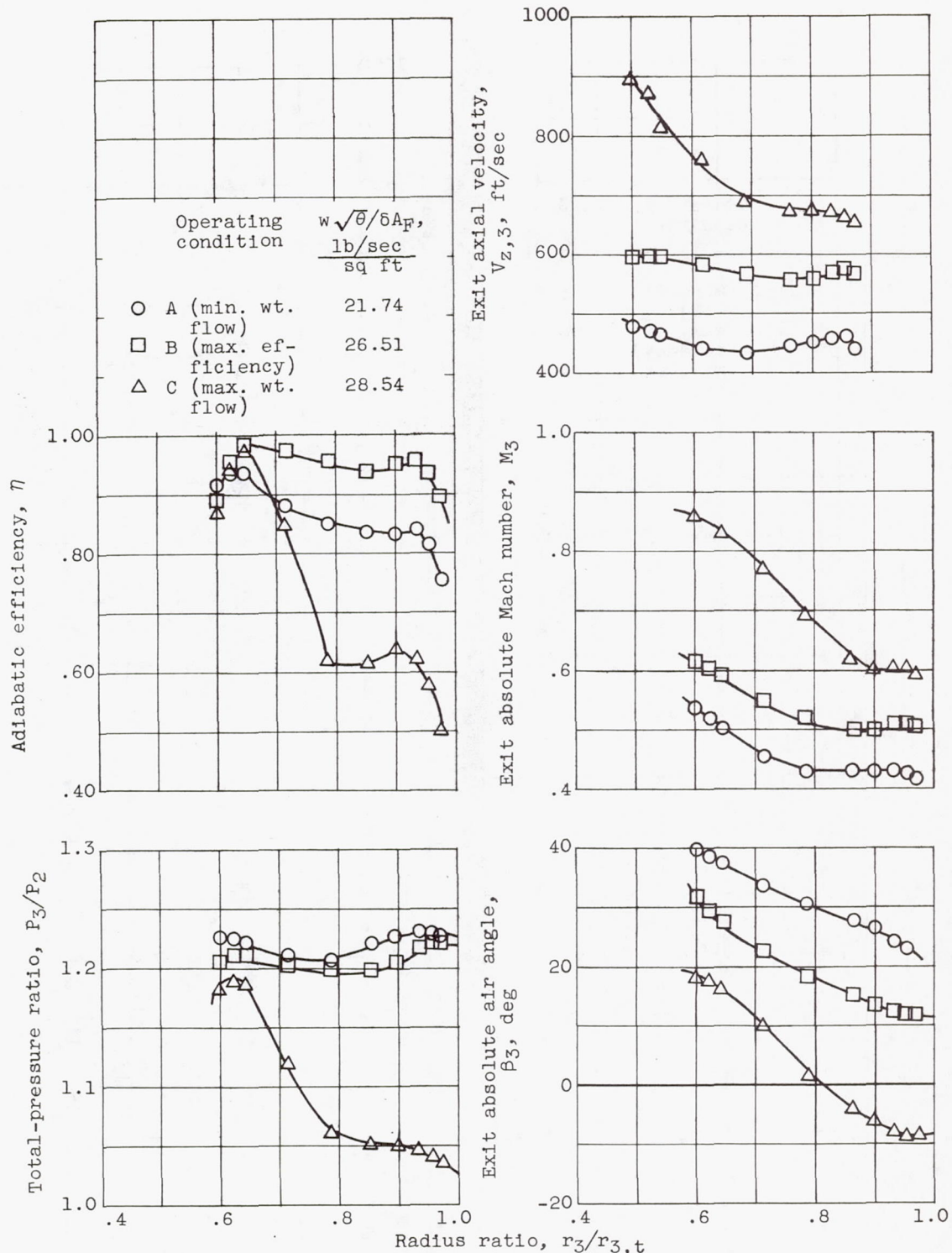
(c) Equivalent speed, 80-percent design.

Figure 8. - Concluded. Outlet conditions for rotor designed with unconventional tangential velocity distribution.

4107



(a) Rotor inlet.                    (b) Rotor outlet.
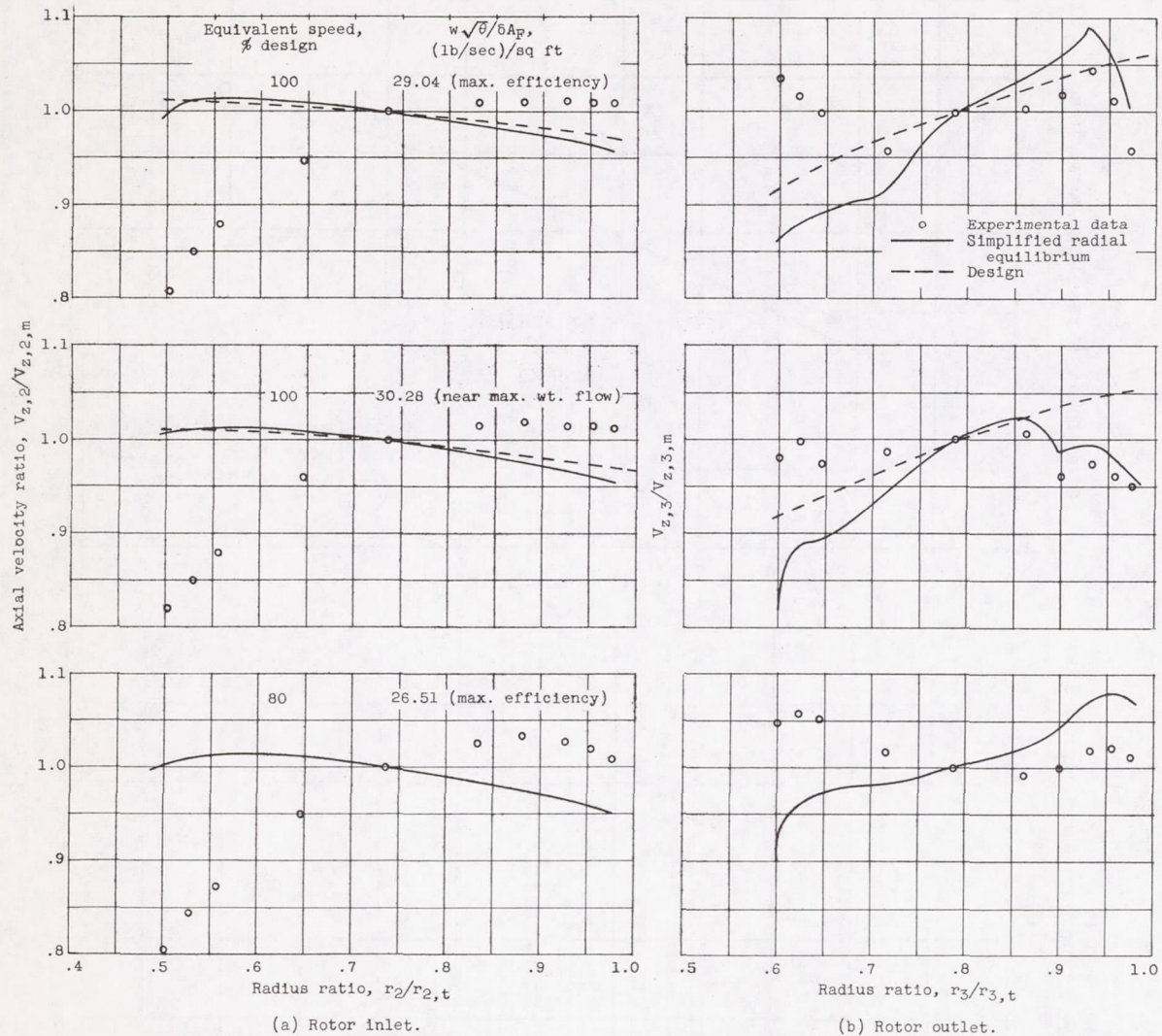
Figure 9. - Radial variation of dimensionless axial velocity computed from simplified radial equilibrium and measured from experimental data.

(a) Rotor inlet.

(b) Rotor outlet.
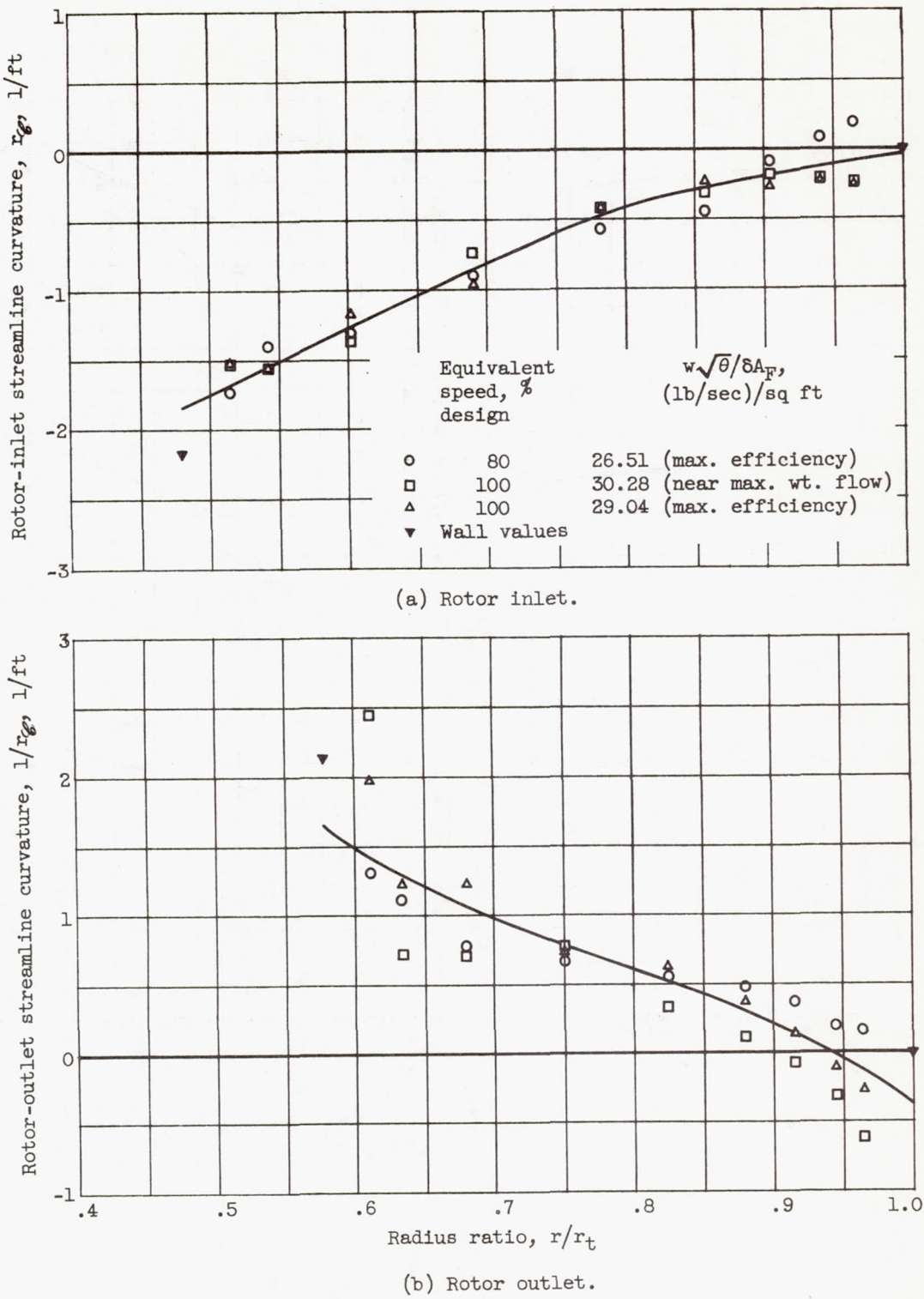
Figure 10. - Radial variations of rotor-inlet and -outlet streamline
    curvature.
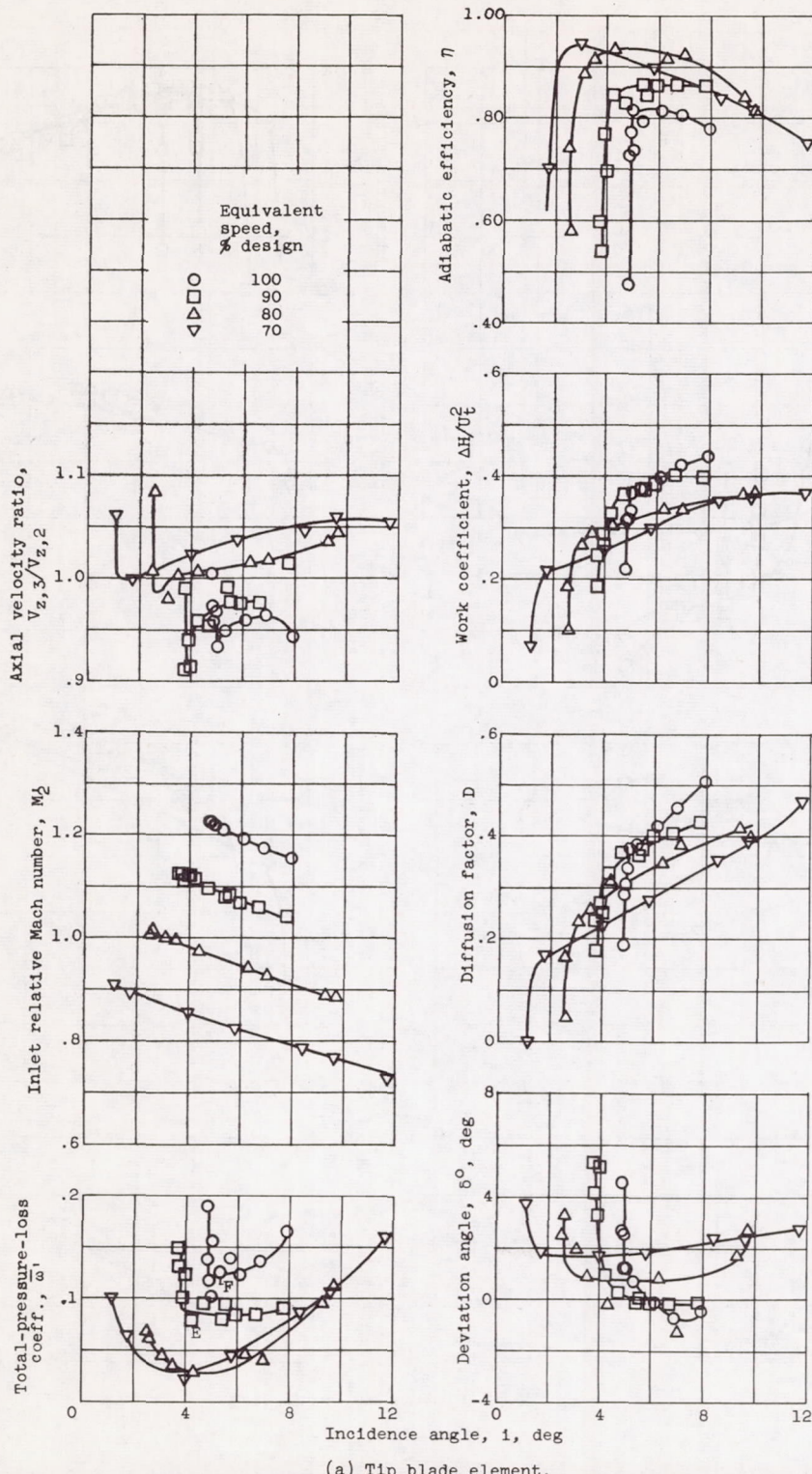
(a) Tip blade element.

Figure 11. - Blade-element performance of rotor designed with un-
conventional tangential velocity distribution.
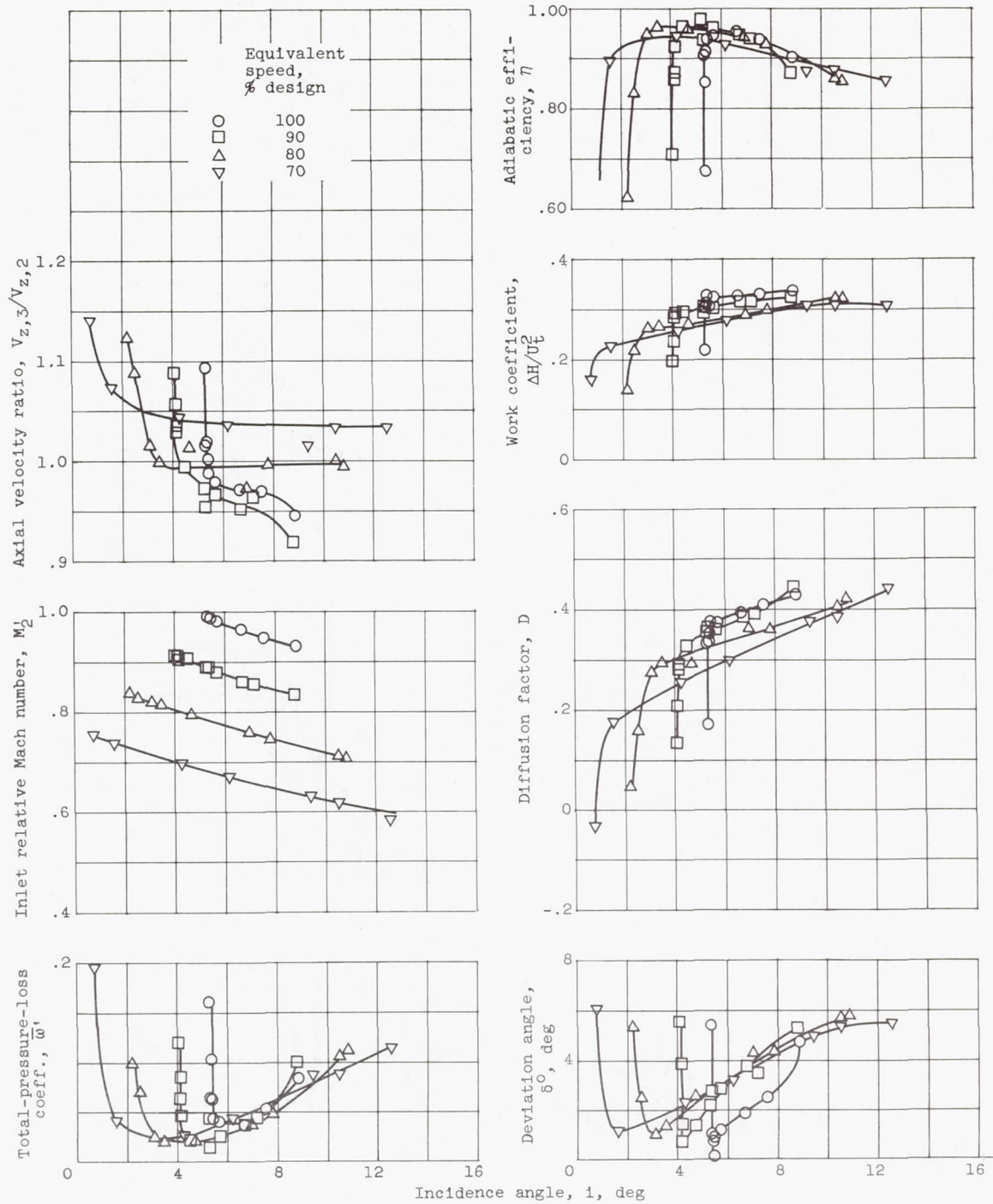
(b) Mean blade element.

Figure 11. - Continued.  Blade-element performance of rotor designed with unconventional tangential velocity distribution.
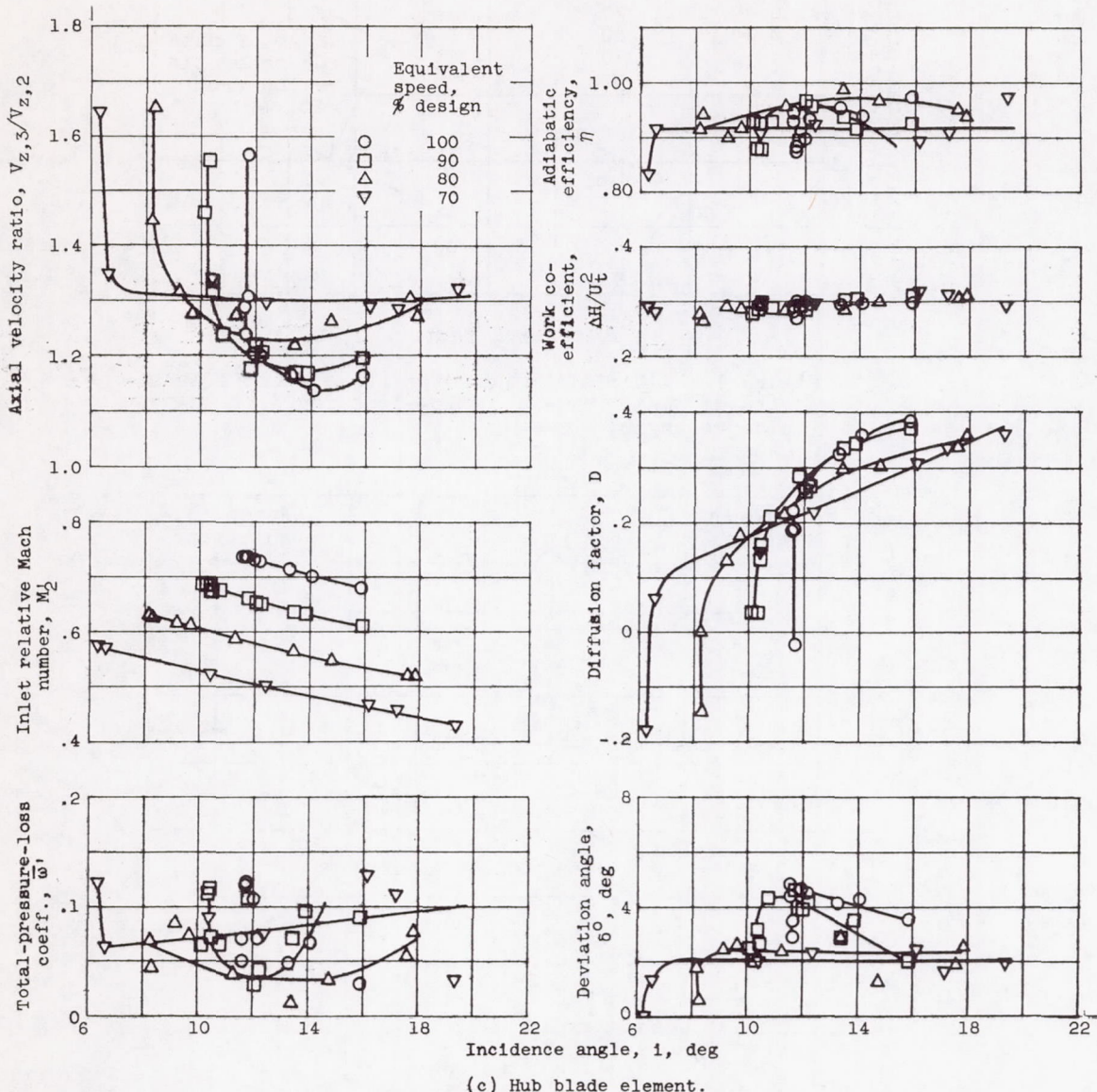
(c) Hub blade element.

Figure 11. - Concluded.  Blade-element performance of rotor designed with unconventional tangential velocity distribution.
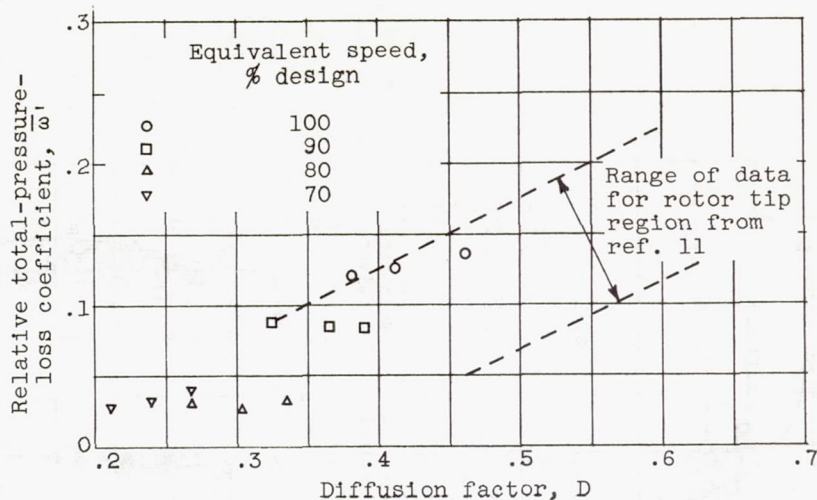
Figure 12. - Variation of rotor tip-element losses with diffusion factor in low-loss range of incidence angle.
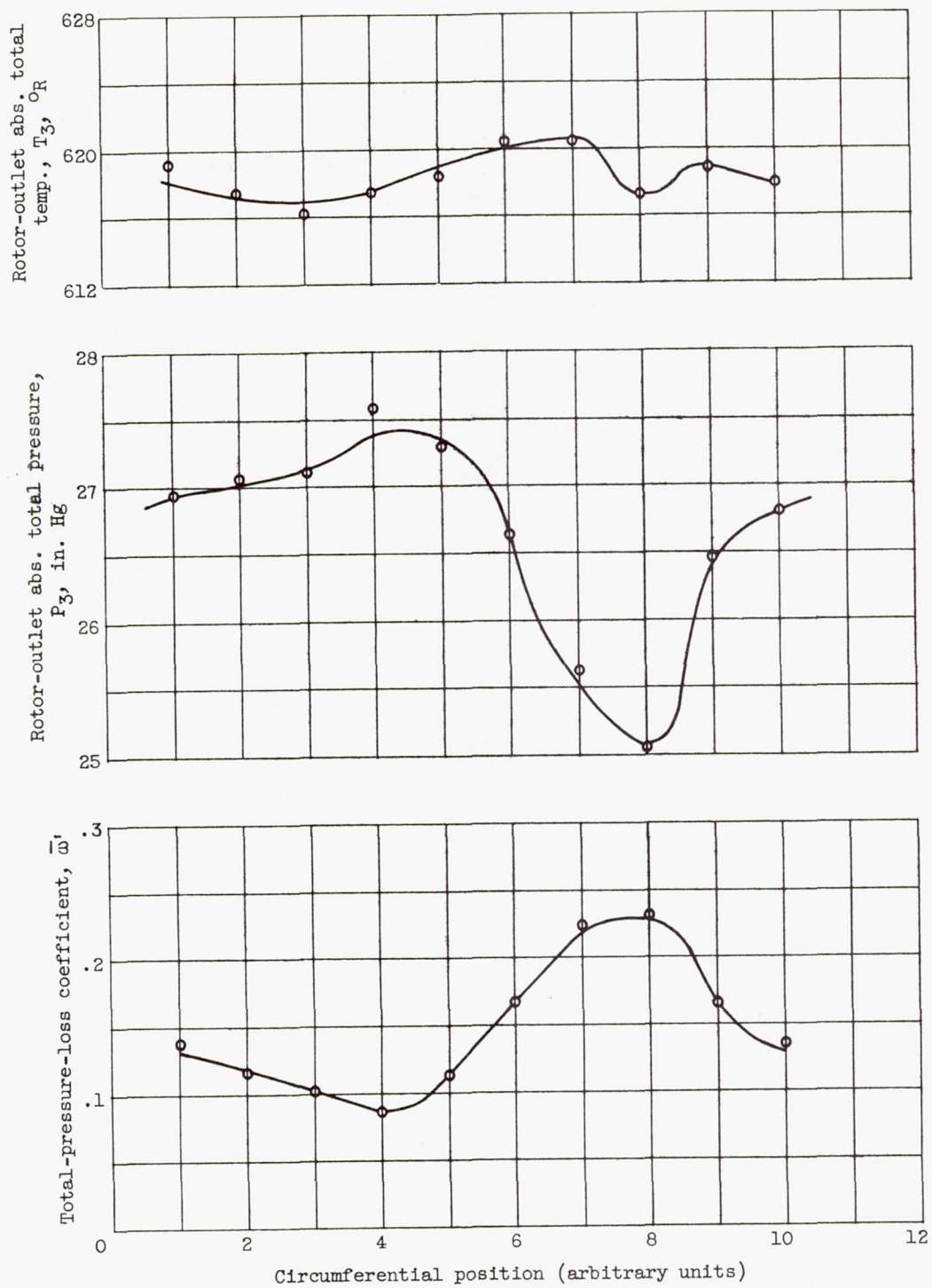


(a) Tip element.

(b) Mean element.

(c) Hub element.
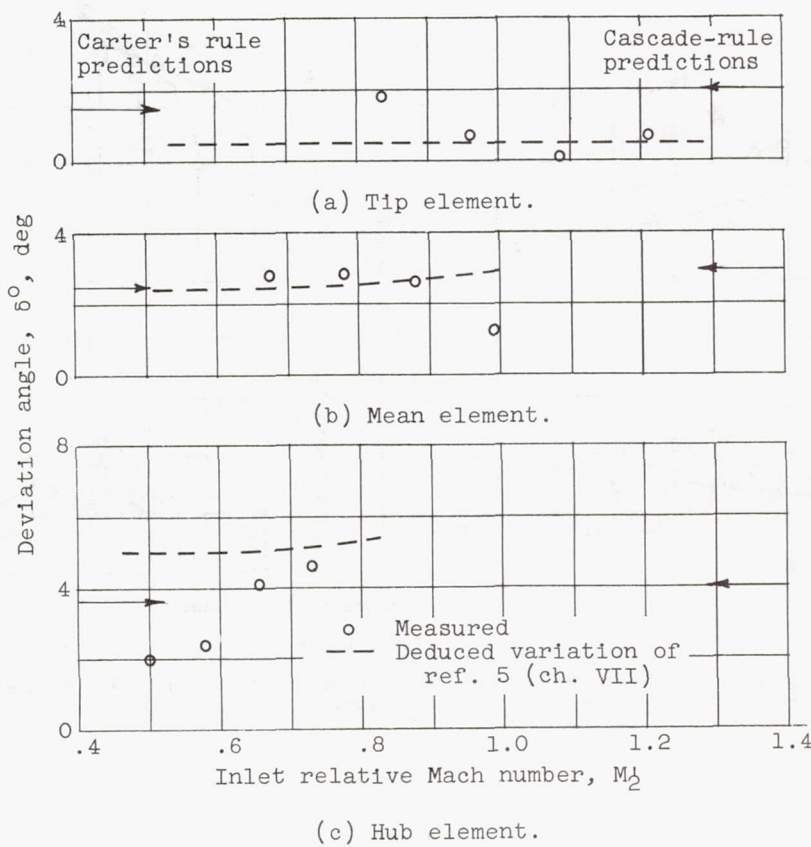
Figure 13. - Comparison of measured deviation angles at minimum-loss incidence angle with values predicted by Carter's rule and deduced variation of reference 5.
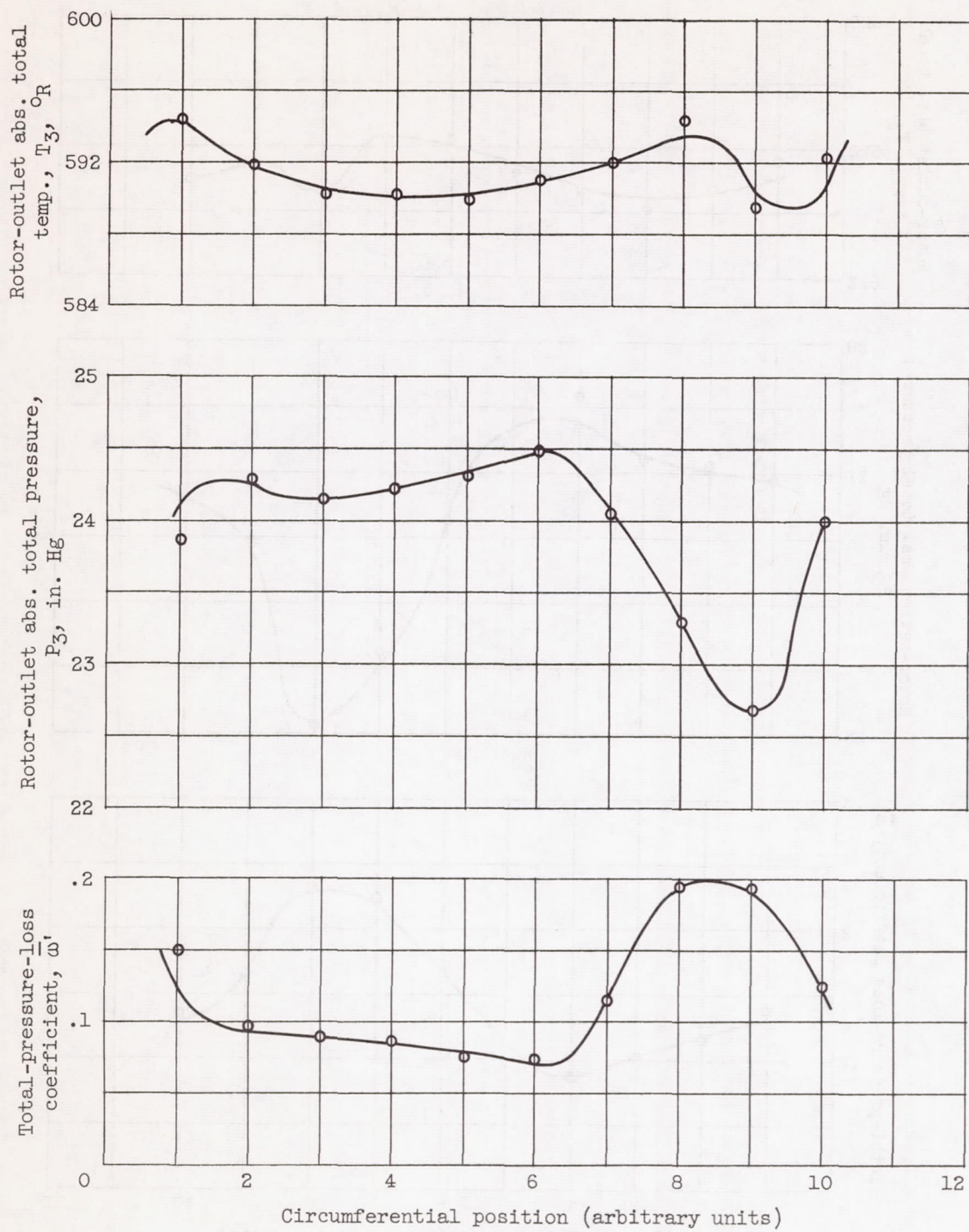
(a) Operating point E (fig. 11(a)).

Figure 14. - Circumferential variations in rotor-outlet absolute total
temperature and pressure and relative total-pressure-loss coefficient
for tip element.

(b) Operating point F (fig. 11(a)).

Figure 14. - Concluded. Circumferential variations in rotor-outlet absolute total temperature and pressure and relative total-pressure-loss coefficient for tip element.
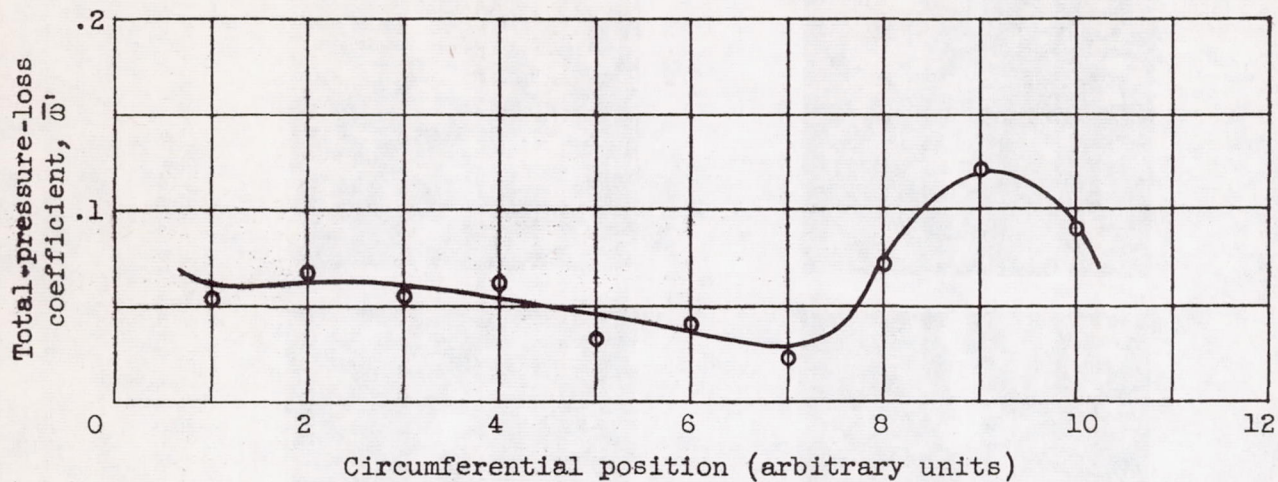
Figure 15. - Circumferential variations of tip-element relative total-
pressure-loss coefficient for operating point E (fig. 11(a)) as meas-
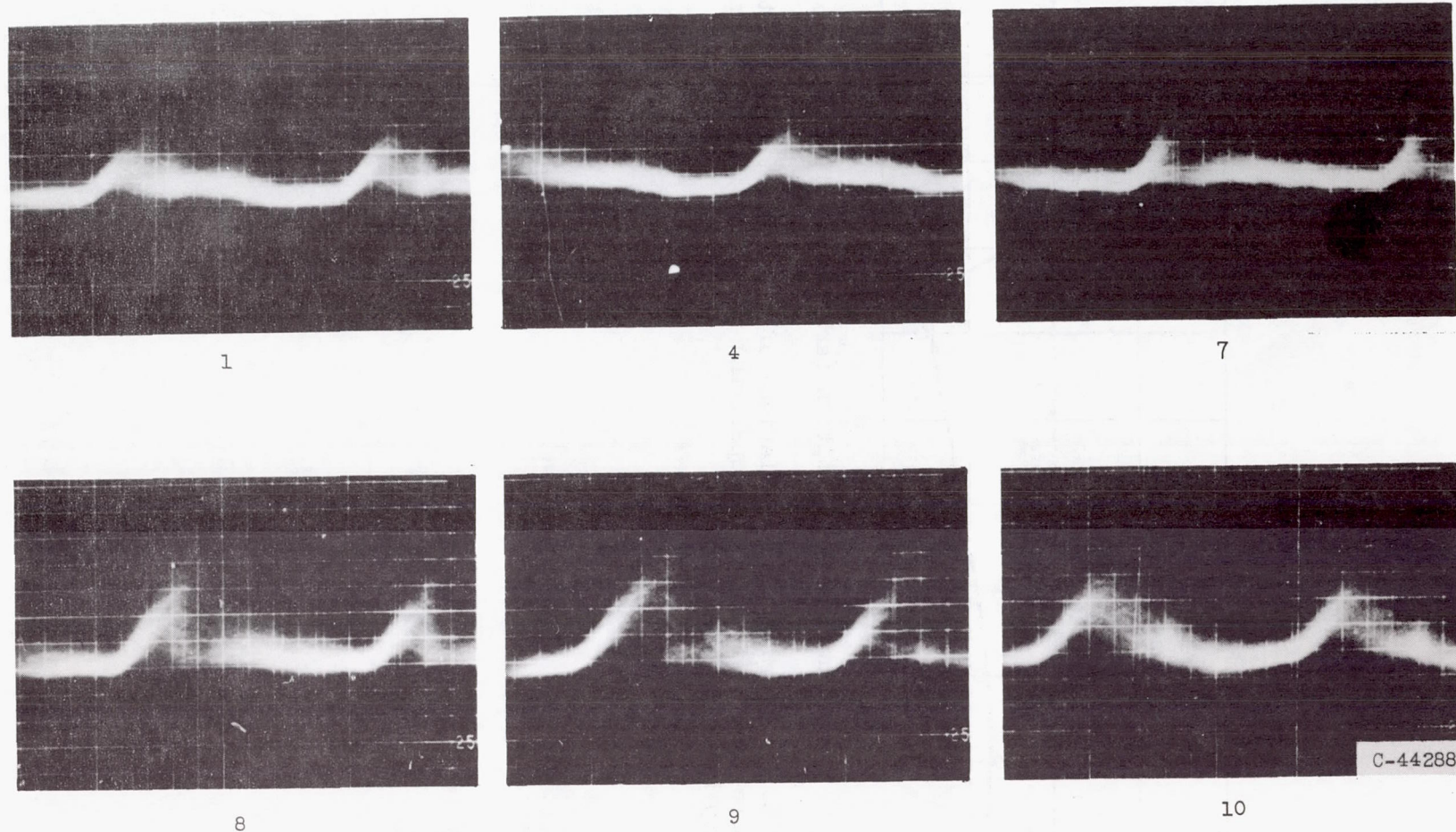ured by hot-wire anemometer.

Figure 16. - Oscilloscope traces of hot-wire-anemometer signal at several circumferential positions for operating point E. (Numbers indicate circumferential positions of fig. 15.)